"BABEŞ-BOLYAI" UNIVERSITY OF CLUJ-NAPOCA

Faculty of Chemistry and Chemical Engineering

Doctoral School of Chemistry

PhD Thesis Abstract

Novel phenothiazine decorated porphyrin derivatives: synthesis, optical properties, protonation study and biological activity assessment

Scientific Advisor:

Prof. Dr. Luminiţa Silaghi-Dumitrescu

PhD Candidate:

Molnár Éva-Andrea

Cluj-Napoca

2022

"BABEŞ-BOLYAI" UNIVERSITY OF CLUJ-NAPOCA

Faculty of Chemistry and Chemical Engineering

Doctoral School of Chemistry

PhD Thesis Abstract

Novel phenothiazine decorated porphyrin derivatives: synthesis, optical properties, protonation study and biological activity assessment

Scientific Advisor:

Prof. Dr. Luminiţa Silaghi-Dumitrescu – *Babeş-Bolyai University, Cluj-Napoca, Romania*

President:

Prof. Dr. Gabriela Nicoleta Nemeş – *Babeş-Bolyai University, Cluj-Napoca, Romania*

Reviewers:

Conf. Dr. Ing. Luminiţa-Camelia David – *Babeş-Bolyai University, Cluj-Napoca, Romania*

Prof. Dr. Bruno Therrien – *Université de Neuchâtel, Switzerland*

Prof. Dr. Ionel Mangalagiu – *Alexandru Ioan Cuza University of Iaşi, Romania*

Cluj-Napoca

2022

Table of contents

Keywords: phenothiazinyl-porphyrins, hyperporphyrins, phenothiazine arms, ethynyl spacer, extended conjugation, fluorescent dyes, skeleton functionality, protonation study

1. General introduction

The systems with extended conjugation are interesting and therefore intensively studied recently due to their electronic properties leading to applications in material science[1,2] or medicine[3,4]. The design of such systems is often based on the potential synergism resulting by the interaction of fragments/molecules already prone to conjugation. Phenothiazines and porphyrins are good candidates for the preparation of extended conjugation systems[5,6], so this thesis presents the results obtained in the study of the synthesis, structural characterization and optical properties of some new phenothiazinyl-porphyrin derivatives.

In the first chapter of the thesis a literature overview on phenothiazine and porphyrin derivatives is presented, including different synthetic methods, applications and biological activity of the examined molecules, as well as the first-time synthesis of phenothiazinyl-porphyrins[7].

The second chapter focuses on the original results in the synthesis of star-shaped *meso*-phenothiazinyl-porphyrins (MPP) and their metallo complexes, containing Ni(II), Zn(II), Pd(II) or Cu(II) ions, coordinated in the central cavity of the macrocycle. The protonation behaviors of the MPP derivatives are investigated under acidic conditions, displaying remarkable photophysical properties, due to the nonplanar structural distortions (saddle-distorted porphyrin ring) induced by protonation.

Core- and peripheral functionalization using different synthetic methods are also described for the preparation of the target molecules. Based on Suzuki-Miyaura cross coupling reactions a series of A_4, AB_3 and *trans*-A_2B_2 type phenyl-bridged porphyrin-phenothiazine dyads are discussed, along their potential applications in cellular staining of human ovarian tumors.

The synthesized new MPP derivatives are fully characterized by 1D, 2D-COSY, 2D-HMQC and 2D-HMBC NMR spectroscopy, respectively HRMS spectrometry, using APCI or ESI ionization techniques. Their photophysical properties including UV-Vis linear and nonlinear absorption and fluorescence emissions are studied in solution and/or solid state.

2. Literature review

2.1. Phenothiazine derivatives

2.1.1. Introduction and background of phenothiazines

Phenothiazines are stable, widely available and nontoxic crystalline solids, which contains 16π electron systems with a tricyclic scaffold and a side chain extending from the middle ring moiety[8]. The phenothiazine core's unique structural features include a "butterfly" type nonplanar conformation, which impedes the formation of ground state aggregates and excimers[9]. The molecular configurations of phenothiazines are between planar and tetragonal folded. In the tetragonal configuration the nitrogen and sulfur atoms are in the sp^3 hybridization state, and the planes containing the benzene rings are folded along the axis passing through nitrogen and sulfur[10].

The chemical structure of phenothiazines provides a significant molecular template for the development of agents able to interact with a wide variety of vital processes[11]. The biologically active phenothiazine derivatives are mostly substituted at position 10 with alkyl-, acyl-, aminoalkyl groups and additionally at position 2 with electron-withdrawing, lipophilic functional groups (ex. -Cl, $-CF_3$). There are used in medicinal chemistry for their neuroleptic[12], antihistaminic[13], antibacterial[14], antifungal[15], antiviral[16] and anti-inflammatory[17] properties. Examples of usually applied phenothiazines include chlorpromazine, trifluprомazine, perphenazine and promazine[18]. Chlorpromazines are primarily used as a neuroleptic to treat symptoms of psychosis.

In additional, phenothiazine derivatives are successfully applied as photoactive materials in organic electronic devices[19] (such as OLEDs and OFETs), batteries, sensors[20], dyes[21], pesticides[22], antioxidants[23] and redox active molecular wires for material science investigations[24]. Due to their strong electron-donating ability (*p*-type building block) and non-planar butterfly conformation, phenothiazines have been widely used in organic photovoltaic (OPV) cells, thin film field effective transistors (FET) and light emitting diodes (LEDs)[25]. Furthermore, phenothiazine-based donor-acceptor type molecules with a variety of π-spacers are common design moieties for dye-sensitized solar cells (DSSC)[26,27].

2.1.2. Functionalization reactions of phenothiazine derivatives

New derivatives of phenothiazine can be obtained by modification of 10*H*-phenothiazine structure in different ways: an introduction of a new substituent at the nitrogen atom (at position 10) or at a carbon atom of the benzene ring (at positions 1-4 and 6-9); an oxidation of the sulfide

into sulfoxide and sulfone functional groups and a substitution of one or both benzene rings with homo- and heteroaromatic rings (ex. azine rings)[28].

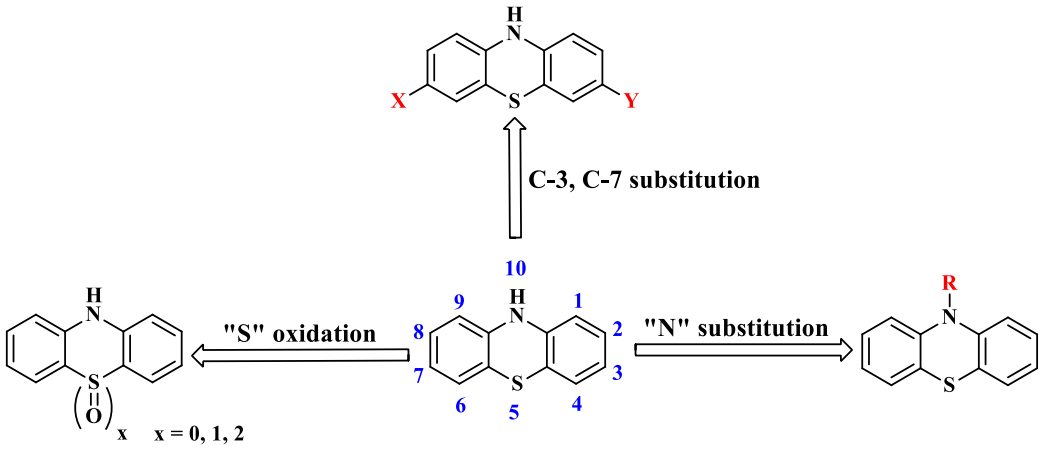

Figure 1. Molecular structure and the key functionalization of 10H-phenothiazine[9]

The presence of electron-rich nitrogen and sulfur atoms significantly enhances the electron-donating character of the phenothiazine unit, which support the electrophilic substitution reaction at C-3 and C-7 positions[29]. The N-10 active site attached with alkyl, aryl, oligo or aralkyl groups to modify the degree of crystallinity, and/or to achieve the desired solubility in organic solvent and solution-processing properties[30]. Similarly, S-heterocycles can be easily oxidized/reduced to achieve sulfur in different oxidation states (sulphide, sulfoxide and sulfone) and to affect the redox and spectroscopic properties[31].

Due to the versatility of its core, the strong electron-donating character and the tunable redox properties, the phenothiazine molecules are well suited for constructing “donor-acceptor” or “push-pull” materials. The functional positions of phenothiazine core (N-10, C-2, C-3, C-7, C-8) typically participate in chemical reactions like halogenations, oxidation, formylation and N-substitution. Particularly, the halogenation at C-3 and C-7 positions generates the precursor materials for the cross-coupling reactions and opens the synthetic pathways for the construction of diverse π-conjugated materials. For this purpose, mono- and poly functionalized phenothiazine derivatives were chosen and different synthetic methods were applied for the synthesis of the target phenothiazinyl-porphyrin molecules.

As carbonyl derivatives are very good starting materials or intermediates in organic synthesis the formylation of phenothiazine is an important reaction. Vilsmeier-Haack reaction or indirect

method via organo-lithium derivatives and subsequent formylation with DMF are two of the methods of choice.

One of the most efficient methods to introduce a formyl group at the phenothiazine core is based on Vilsmeier-Haack reaction, which was applied first on 10-methyl-phenothiazine by Buu-Hoi and Hoan[32]. They obtained 3-formyl-10-methyl-phenothiazine in one step procedure using N-methylformanilide and $POCl_3$ as formylating agent. The reaction of a formamide derivative and phosphoryl chloride resulted initially a chloromethyliminium salt, also called the Vilsmeier complex, which are used as the electrophile in electrophilic substitution reaction with the activated aromatic substrate[33].

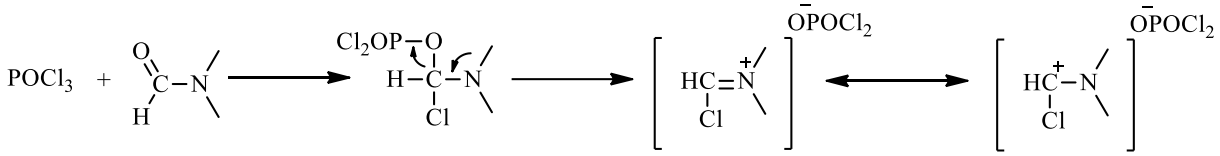

Scheme 1. Vilsmeier-Haack formylation reagent

The palladium-catalyzed cross-coupling reactions are developed as a mild reaction procedure for derivatization of the phenothiazines in good to excellent yield. The coupling reactions are used as an efficient method to introduce new fragments to the phenothiazine core with major influences on the extended π-conjugated system. According to the literature, a large number of π-conjugated donor-acceptor (D-A) or push-pull phenothiazine molecular systems are explored for various applications in optoelectronics[34]. A vast array of methodology options became accessible taking into consideration that phenothiazine derivatives can be successfully used as coupling partners in Suzuki-Miyaura, Heck and Sonogashira reactions.

2.2. Porphyrin derivatives

2.2.1. Introduction and background of free-base and metalloporphyrins

Porphyrins, also called "pigments of life"[35], are important class of tetrapyrrolic compounds with many biological representatives including chlorophylls (centerpiece of photosynthesis), hemes (key molecules for biocatalysts and oxygen transport in blood), cytochromes (proteins containing heme in oxidation-reduction reactions), peroxidases (enzymes in various biological processes) and others.

Porphyrins are an 18π heteroaromatic macrocyclic compounds that consists of four pyrrole units and four interpyrrolic methine bridges in a planar conformation. The systematic naming

based on the 1-24 numbering system is adopted from the corrinoid nomenclature and is later accepted by the International Union of Pure and Applied Chemistry (IUPAC) and International Union of Biochemistry (IUB). If the fundamental porphyrin framework is substituted at the *meso* (5, 10, 15, 20) and/or *β*-positions (2, 3, 7, 8, 12, 13, 17, 18) with non-hydrogen atoms or groups and two of the inner nitrogen atoms (21, 23) are protonated, the resulting compounds are known as free-base porphyrin (*Figure 2a*). The positions where the four pyrrolic sub-units linked on opposing sides are identified as α-positions (1, 4, 6, 9, 11, 14, 16, 19)[36]. The aromaticity (following Hückel's (4n+2)π rule) has been well determined by its chemical and physical properties. Originally there are 22π electrons but only 18 are delocalized[37] (*Figure 2b)*.

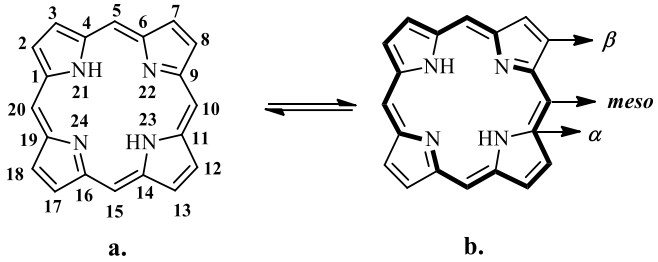

Figure 2. Porphyrin molecular structure and nomenclature

Due to this strong conjugation, porphyrins have unique electronic and optical properties, good stability and conformational flexibility, which allow their multiple applications in modern scientific fields[38], such as photosensitizers for photodynamic therapy[39], chemosensors[40], near-infrared dyes[41], molecular wires[42], light harvesting arrays[43], unidimensional conductors and semiconductors[44], nonlinear optical materials[45], nanomaterials[46], and so forth.

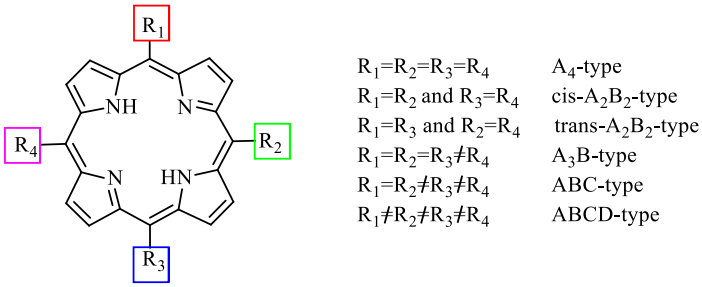

Figure 3. Different type of meso-substituted-porphyrins

To achieve these special functions, design and synthesis of structurally varied porphyrin derivatives is necessary. Most applications require unsymmetrically substituted derivatives, thus the interest of *meso*-substituted porphyrins with mixed type of substituents are highlighted.

Generally, the target molecules are members of A_x- and ABCD-type series[47]: A_4-type[48], *cis*- and *trans*-A_2B_2-type[49], A_3B-type[50], ABC-type[51] and ABCD-type[51] (*Figure 3*).

The *meso*-substituted porphyrins are prepared according to one of two methods: mixt condensation reaction of pyrrole with aromatic or aliphatic aldehyde and subsequent oxidation of obtained porphyrinogen to corresponding porphyrin in one-pot, or condensation cyclization reaction of pyrrole with aldehyde, followed by the oxidation of porphyrinogen to porphyrin with different oxidizing agents, in a separated step[52].

The synthesis of symmetrical substituted *meso*-porphyrins was reported first by Rothemund[53] in 1936, using a simple condensation of pyrrole and acetaldehyde, dissolved in pyridine/methanol, in a sealed tube.

Adler[54] observed, for the first time, that the yields are significantly better when the reaction occurs in acidic media. He and co-workers modified the synthesis of *meso*-substituted porphyrins mixing equimolar amounts of pyrrole and benzaldehyde in presence of propionic acid to give the corresponding derivatives directly precipitate with yields of ~20%.

A new strategy for the synthesis of *meso*-substituted porphyrins under mild conditions was extended by Lindsey[55] in a two-step reaction. The condensation of pyrrole with aryl aldehyde was carried out in chlorinated solvents (CH_2Cl_2, $CHCl_3$) with strong Lewis acids as catalysts (TFA or BF_3*Et_2O), under inert atmosphere. In this case, the oxygen from air is not sufficient to oxidize the obtained tetra-arylporphyrinogen, so a high potential oxidizing agent (quinines, chloranil or DDQ) could be used to achieve the porphyrin macrocycle up to 35% yield (A_4-type).

A strategy for the synthesis of asymmetrically substituted porphyrins was introduced by MacDonald[56] in 1960. This “2+2” methodology is successfully used in the preparation of *trans*-*meso*-substituted porphyrins (A_2B_2-type), and the synthetic route is based on the condensation reaction of a dipyrromethane and an aldehyde in presence of an acid catalyst to give the porphyrinogen intermedier, followed by an oxidation, usually with an electron deficient quinone, to affords the corresponding porphyrin derivative[57].

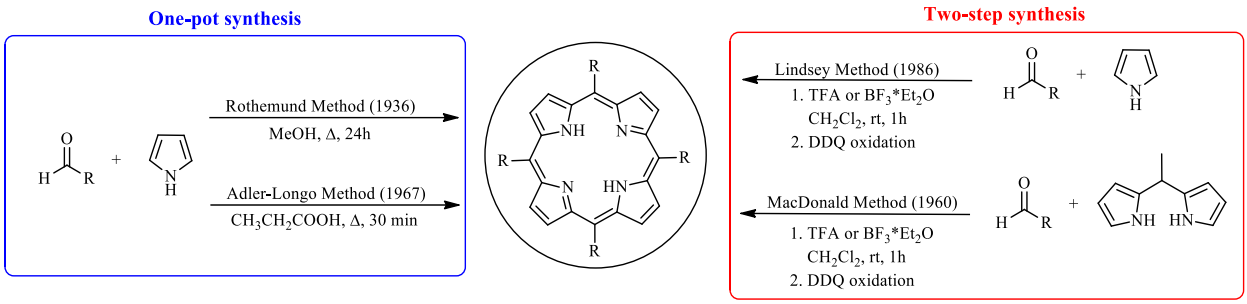

Figure 4. Methods for the synthesis of meso-substituted porphyrins

Generally, porphyrins are prepared in a metal-free form (free-base porphyrins), but they have a size-limited conjugation cavity for binding of various metal ions, forming metalloporphyrins[58]. The desired metal ions are successively inserted in a two-step reaction: the coordination (preequilibrium) step of two pyrrolenine nitrogens to obtain an intermediate, and the deprotonation step of the established complex to form the metalloporphyrin.

Metalloporphyrins usually create square-planar coordination with the central metal ion in the plane of the four pyrrole nitrogens, but occasionally the metal may be five-coordinate with square-pyramidal geometry, six-coordinate with distorted octahedral geometry or eight-coordinate to generate a sandwich compound with square antiprism geometry[59].

Due to the charge, size and spin multiplicity of metal ions, there are two types of metalloporphyrins: *regular (in-plane) complexes*[60], when the size of metal ion is appropriate to be inserted into the center of the planar ring system and the resulted new metal-nitrogen bonds are between 55 and 80 ppm or *sitting-atop (out-of-plane) metalloporphyrins*[61,62], in which case the ionic radius is too large to fit into the center of the macrocycle (over 80-90 ppm) and are located out of the plane containing the four pyrrolic nitrogens, distorting it. The most typical distorsions are saddle, ruffled, wave (chair-like) and dome, arising from the strong interaction between the porphyrin core, the peripheral substituents and the central metal ion (*Figure 5*)[58]. The manipulation of ligand distortions can modify the physical and chemical properties of porphyrin complexes (redox potential, catalytic activity), due to the symmetry decreases, which caused several spectral changes in the electromagnetic spectrum[63].

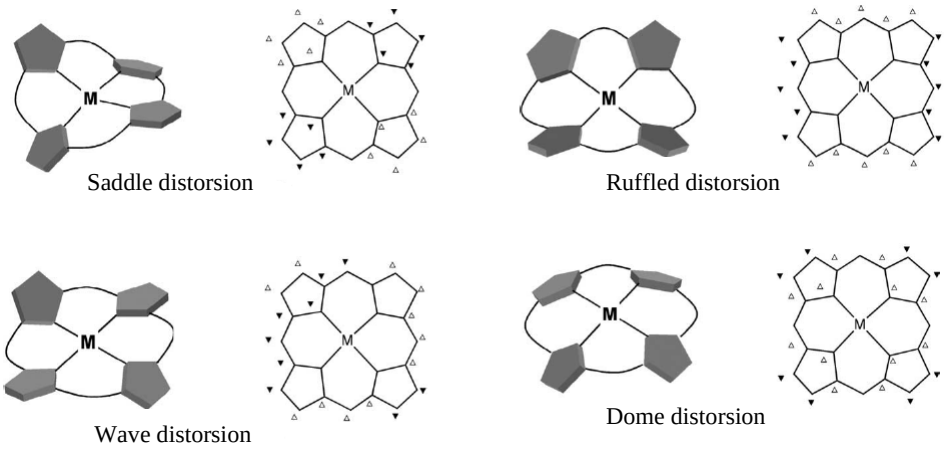

Figure 5. The non-planar distorsion of metalloporphyrins and the deviation of atoms from the mean plane of the porphyrin core: above (▵) and below (▿)[64]

Metalloporphyrins can be prepared using one-pot procedure[65,66] by mixing carboxylic acids (propionic acid, glacial acetic acid) and *m*-nitrotoluene, or Adler two-step method[67]. The advantages of one-pot mixed solvent procedure are the much higher yield, the shorter reaction time and the simpler workup technique compared to the Adler method, which is carried out by incorporation of metal ions into the central cavity of free-base porphyrins in N,N-dimethylformamid (DMF) solution at high temperature. Moreover, in the one-pot mixed solvent method the reflux temperature is lower, which decreases the side effects, and it is valid for different substituted aldehydes[58].

The aromatic character of porphyrins was proved by NMR spectroscopy[68]. The highly conjugated π-electron system causes a strong ring current in the porphyrin macrocycle placed in the magnetic field, and this ring current gives rise to anisotropic shielding of the protons. Due to the anisotropic effect, the NMR signals for the deshielded *meso* protons appear at very low field (δ from 9.7 to 11.2 ppm), the β (pyrrolic) protons are also deshielded (δ from 8.5 to 9.9 ppm), whereas the NH protons, inside the porphyrin ring system, show up at very high field (δ from -1.4 to 4.4 ppm)[69]. In the ^{13}C-NMR spectrum three different zones are observed: the chemical shifts of α carbons appear at 145 ppm, the β carbons around 130 ppm, and the *meso* carbons are generally between 95 and 120 ppm. In the ^{1}H-NMR spectrum of metalloporphyrins the absence of the signal at high field (-3 ppm, inner NH protons) and the upfield shifts of the signals for *meso*-protons, due

to the reduced ring current effects is observed after the coordination to the M^{2+} cations (M=Ni, Pd, Zn, Cd or Mg).

It was identified early that the intense purple color of porphyrins is a consequence of the highly conjugated π-electron system, in 1959 Gouterman[70,71] proposed the four-orbital model that explains the absorption spectra of porphyrins. Based on this theory, the absorption bands in porphyrin molecules origin from transitions between two HOMOs and two LUMOs, two highest occupied π orbitals and two lowest unoccupied π* orbitals. Due to this property, the porphyrin derivatives present characteristic electronic absorption spectra, which contain one intense band (*Soret band*) in the near-ultraviolet region around 420 nm and denotes $S_2 \leftarrow S_0$ transitions, respectively four low-intensity bands (*Q bands*) in visible region between 480 and 650 nm, indicating $S_1 \leftarrow S_0$ transitions[72,73] (*Figure 6a*). The extinction molar coefficient (ε) of the Soret transition is very high, around 10^4-10^5 $M^{-1}*cm^{-1}$.

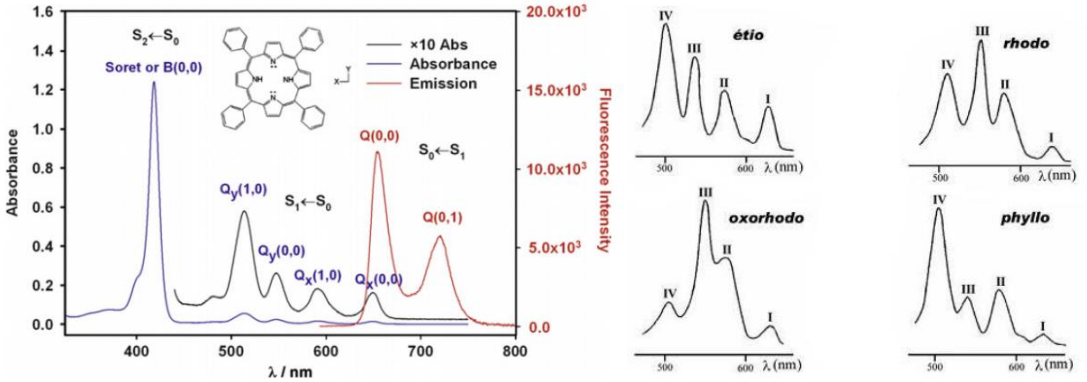

a. **b.**

Figure 6. Typical absorbance and fluorescence spectra of free-base porphyrins (a) and different type of Q bands (b)

The relative intensity and position of peaks are dependent on the type of the substituents at the *meso*- or *β*-positions, as well as on the solvent and concentration. Basing on this consideration, porphyrins Q bands are different form, classified as *etio*, *rhodo*, *oxo-rhodo* and *phyllo*[74] (*Figure 6b*). The *etio*-type is observed in the case of *β*-substituted porphyrins with six or more functional groups, generally alkyl groups ($Q_4>Q_3>Q_2>Q_1$). Substituents with π-electrons (for ex. carbonyl, vinyl) directly linked to the *β*-positions give a *rhodo*-type spectrum ($Q_3>Q_4>Q_2>Q_1$), however when these groups are on opposite pyrrole ring the spectrum is called *oxo-rhodo*-type ($Q_3>Q_2>Q_4>Q_1$). In the case of *meso*-substituted-porphyrins *phyllo*-type spectrum is obtained ($Q_4>Q_2>Q_3>Q_1$)[75]. The fluorescence emission spectra of porphyrins consist of two strong emission

bands, a distinct major peak at 650 nm and another peak around 720 nm (*Figure 6a*). The spectra are characteristic of many free-base porphyrins[76].

After the metal insertion, the Soret band is only slightly affected, but the four Q bands, which are typical of free-base porphyrins, are reduced to two bands (α and β), situated between 500 and 600 nm, due to the D_{4h} symmetry of regular, coplanar metalloporphyrins[77]. *Regular metalloporphyrins*, which contains closed-shell metal ions (d^0 or d^{10}), have a little effect on the porphyrin π-π^* energy gap, due to the metal-based orbitals low energy level. On the other hand, *hyperporphyrins*, in which the metals are of $d^{6\text{-}9}$, show an increased porphyrin π to π^* orbital interaction, caused by the metal to ligand π-backbonding. As compared to the free-base porphyrins, the typical in-plane metalloporphyrins display larger blueshifts in the Soret-range, while the out-of-plane derivatives show small blueshift, accordingly to the increasing and decreasing energy gaps between the excited and ground states.

2.2.2. Cross coupling reactions of porphyrins

Cross-coupling reactions represent a new way of synthetic transformations by combination of an organometallic reagent (organoboron, organosilicon, organotin, organozinc…) with an organic electrophile (halides, pseudohalides…), in the presence of metal catalyst (from groups 8-10) to form new C-C, C-H, C-N, C-O, C-P, C-S or C-M bonds[78].

A general catalytic cycle for coupling reactions involves a sequence of *oxidative addition*, which is often considered as the rate-determining step, *transmetallation* and *reductive elimination* (*Figure 7*). The carbon-heteroatom cross-coupling reaction with porphyrin halides includes a palladium catalyst, a ligand, an aryl halide, a soft nucleophile, a base and the solvent. In the first reaction step a bulky, unsaturated palladium catalyst is oxidized from palladium(0) to palladium(II) and is coupled with alkyl halide to form an organopalladium complex (see complex B). Then complex B undergoes transmetallation with a base-activated nucleophile to yield a new palladium(II) complex (see complex C). The final step is the reductive elimination, where the organopalladium species (complex C) releases the coupled-porphyrin product and regenerates the palladium(0) catalyst.

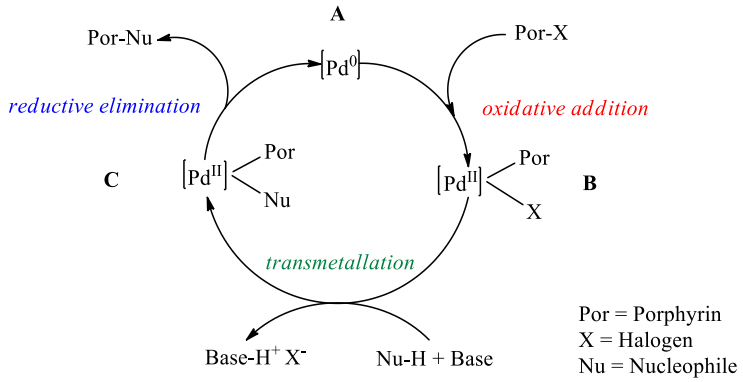

Figure 7. General catalytic cycle for cross-coupling reactions of haloporphyrins[79]

The catalytic use of electron-rich ligands in combination with palladium precursors has a positive impact in all the cross-coupling reaction. The role of bulky phosphine ligands is to stabilize the Pd(0) intermediates and avoid its precipitation[80]. The potential reaction solvents include: non-polar, non-coordinating solvents (benzene and toluene), polar, coordinating solvents (THF, DME, DMSO, DMF), polar, protic solvents (methanol, ethanol, water), as well as solvents mixture to optimize the solubility of the substrates.

Postfunctionalization of porphyrins can be classified into two classes: *core-functionalization*, when the core-skeleton of macrocycle is directly modified at the *meso*- or *β*-positions and *peripheral-functionalization*, when the new substituents are introduced on the peripheral arms[81] (*Figure 8*). In these cases, the functionalization reactions are realized using substituted porphyrins with alkynes, halogens and metals on the porphyrin core or the peripheral part. The most of these functionalizations are realized using different *cross-coupling reactions*, namely the application of transitions metal catalysis is an efficient strategy in the synthesis of more elaborated porphyrin systems.

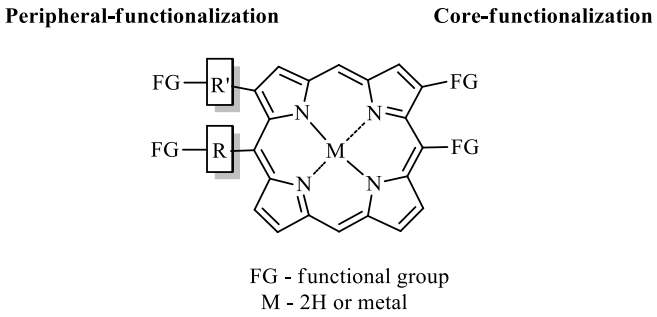

Figure 8. Classification of porphyrin functionalization by position

By transition metal catalysis the direct modification of *meso*- and *β*-carbons can occur with high efficiency, high selectivity and environmentally-friendly processes, while another advantage is to reduce the multistep synthesis, which is not achievable by conventional methodologies. Most of the cross-coupling reactions are based on Pd-catalyzed methods, which include Mizoroki-Heck reactions[82,83], Suzuki-Miyaura couplings[84,85], Negishi couplings[86], Migita-Kosugi-Stille reactions[87], Sonogashira couplings[88,89,90] and Buchwald-Hartwig aminations[91,92]. In addition, the palladium-mediated transformation is a successfully application to derivatize halogenated porphyrins at different *meso*- and *β*-positions with highly effective manner. Due to these beneficial properties, the Suzuki and Heck reactions are the most widely used transition metal catalyzed coupling techniques for the synthesis of π-conjugated porphyrin arrays (for ex. *meso-meso*, *meso-β* and *β-β*-linked porphyrins)[93,94].

Suzuki-Miyaura coupling reactions

The Suzuki-Miyaura cross-coupling reactions between organoboron compounds and organic halides, pseudohalides or triflates in the presence of a palladium catalyst and a base, provide an efficient method for the construction of new carbon-carbon linkages[95,96]. The benefits of palladium-mediated cross-coupling reactions include the availability of the organoboron reagents, which are inert to water, related solvents and oxygen, the mild reaction conditions, thermal stability and low toxicity of starting materials[97]. Moreover, the obtained by-products are also non-toxic and easily extracted from the mixture, thereby making the Suzuki-Miyaura reactions scalable and cost-effective for industrial processes[98].

As previously mentioned, the catalytic cycle contains three steps: starting from *oxidative addition* of organic halide and Pd(0) catalyst to form an organopalladium complex, which interaction with a base and a boronic acid derivative gives an organopalladium species via *transmetallation*, while the desired cross-coupling product be obtained by *reductive elimination*, which reconstructs the Pd(0) catalyst and completes the catalytic cycle[99]. The commonly applied catalysts are the tetra-coordinated palladium-phosphine complexes such as $Pd(PPh_3)_4$, $Pd(PPh_3)_2Cl_2$, $Pd(dppf)Cl_2$ or $Pd_2(dba)_3$[100], while the most frequently used bases are Cs_2CO_3[101], K_2CO_3[102], KO*t*Bu[103], K_3PO_4[104], NaOH[105] and NEt_3[106].

The Suzuki-Miyaura reaction is an efficient tool for the construction of large macrocyclic architectures based on *meso*- or *β*-substituted porphyrins, due to the good reactivity of haloporphyrin derivatives.

Mizoroki-Heck coupling reaction

The Mizoroki-Heck coupling[107] is a chemical reaction of aryl halides (or triflates[108], aryl halides diazonium salts[109], sulfonyl halides[110]) with alkenes in presence of Pd(0)/Pd(II) catalysts and a base to afford substituted alkenes. It is an effective carbon-carbon bond forming method, which is widely used in industry.

The coupling reaction is catalyzed by palladium salts or complexes, such as $Pd(PPh_3)_4$, $PdCl_2$, $Pd(OAc)_2$, the supporting ligands mostly are PPh_3 or BINAP, while the generally applied bases are TEA, K_2CO_3 and NaOAc[111,112,113]. The catalytic cycle begins with an *oxidative addition*, in which step the Pd(0) catalyst (generated in situ from Pd(II) precursor) inserts in the aryl to bromide bond and forms a π-complex with the alkene component. After the palladium-carbon *syn addition* step, the *beta-hydride elimination* generated a new palladium-alkene π-complex, which is destroyed in following section, forming the desired alkene derivative and the Pd(0) catalyst by *reductive elimination* of the Pd(II) precursor by a corresponding base[114].

The Mizoroki-Heck reactions are the most widely used coupling technique for the synthesis of unsaturated porphyrin structures, many of which are important building blocks in the construction of more elaborated systems.

2.2.3. *Meso*-phenothiazinyl porphyrins

The *meso*-phenothiazinyl-porphyrins (MPP) are azaheterocyclic systems based on arrays of (hetero) aromatic units and phenothiazine chromophores directly linked to the porphyrin core7. A series of linear π-conjugated oligomers, including oligophenothiazines, have been introduced to the porphyrin core to create star shaped porphyrins, which are good candidates as fluorescence emitting materials[115].

The D-π-A or push-pull structures are the typical structural designs for efficient porphyrin dyes and these types of compounds support charge transfer from electron donating moiety to porphyrin acceptor[116]. Porphyrin dyes with π conjugated systems, such as phenothiazines, have received remarkable attention as sensitizers in photonic devices (ex. DSSC applications), due to their high molar absorption coefficients, stability and ease of structural modification via peripheral

substitutions. Furthermore, phenothiazine has been widely used in optoelectronics as a donor segment, due to the existence of electron-giving sulfur atom and has a better electron-donating ability than generally used amine-type dyes (*Figure 10a)*[117,118]. The star shaped porphyrin chromophores bearing two or more phenothiazine or diphenothiazine arms in the *meso*-position can emit intense red light with fluorescent quantum yield higher than most porphyrins reported, indicating the phenothiazine ring as a good building block for impeding the aggregation and intermolecular excimer formation owing to its butterfly structure in the ground state[7,115,119].

Moreover, the properties of the porphine macrocycle to aggregate in the body fluids and tissues, explain the continuous interest for the synthesis of new porphyrin derivatives with enhanced photodynamic effect on target cells[120]. A comparison between the photochemical properties of porphyrin and phenothiazine molecules, emphasize their potential application as functional dyes in photodynamic therapy (PDT). *In vitro* photosensitization experiment of some *bis*- and *tris*-aryl-MPPs show variable photodynamic effect in correlation with the concentration, cell lines (HaCaT and A431 human skin cells) and irradiation wavelengths applied. In case of *tris*-aryl-MPPs, the irradiation with blue light reduced significantly the viability of tumoral cells, while *bis*-aryl MPP derivatives showed no photosensitizer properties upon irradiation with neither blue nor red light. Furthermore, *tris*-aryl-MPP (*Figure 9b)* showed increased phototoxicity after exposure to red light, which property highlighted the fact that the MPPs are potential candidates for photodynamic therapy, because longer wavelength penetrates the tissues deeper, making an enhance PDT effect[7].

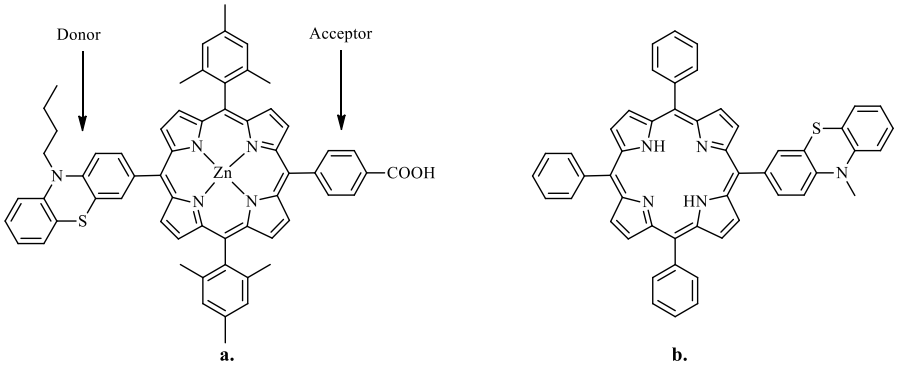

Figure 9. Molecular structure of trans-A_2BC[117] (a) and A_3B[7] (b) meso-phenothiazinyl-porphirins

Consequently, the peripheral phenothiazinyl substituents can impart the desired chemical characteristics to the porphyrin macrocycle, showing interesting photophysical and electrochemical properties, medical treatment[121], photosensitisers and wide range of different

technology[122]. The multiple functionalization possibilities of the highly stable planar macrocyclic porphyrin core combined with the electron rich phenothiazine unit results promising properties and high impact on the optical performances of the porphyrin-based materials. The star shaped *meso*-tetraaryl-porphyrins with one or more neutral phenothiazine arms are good candidates for photoinduced energy transfer systems ("push-pull" porphyrin), as well as biologically active compounds for potential application in PDT of cancer.

These properties prompted me to design and synthesize new *meso*-tetraarylporphyrin derivatives with peripheral phenothiazine units (from one up to four), and to study their structure-photophysical properties relationship by both experimental (absorption and emission spectra) and theoretical methods (DFT calculation). The new MPP and metalloMPP derivatives, with extending linear π-conjugation may open new perspectives for further application.

3. Original contributions

3.1. Synthesis of phenothiazine precursors, NMR and mass spectra study

This part of thesis presents a series of phenothiazine precursor which was prepared for the synthesis and postfunctionalization of new phenothizinyl-porphyrin derivatives. The synthetic pathway includes three reaction steps: first the N-alkylation of heterocyclic nitrogen, followed by the formylation of the phenothiazine core and functionalization of N-alkyl- or N-alkyl-3-formyl-phenothiazine by different cross-coupling reactions.

3.1.1. N-alkyl-10*H*-phenothiazines

10-methyl-, 10-(6-bromohexyl)- and 2-chloro-10-methyl-phenothiazine were prepared by a modified method originally recommended by Buu-Hoi[32] in 1951: to a suspension of $NaNH_2$ or NaH in THF was added slowly 10*H*-phenothiazine, respectively 2-chloro-10*H*-phenothiazine, solved in THF, under inert atmosphere. The obtained 10-Na-phenothiazine was subsequently reacted with an alkyl iodide (methyl-iodide) or bromide (1,6-dibromohexane) to form the corresponding 10-alkyl-10*H*-phenothiazine derivative, as white crystals (*Scheme 2*).

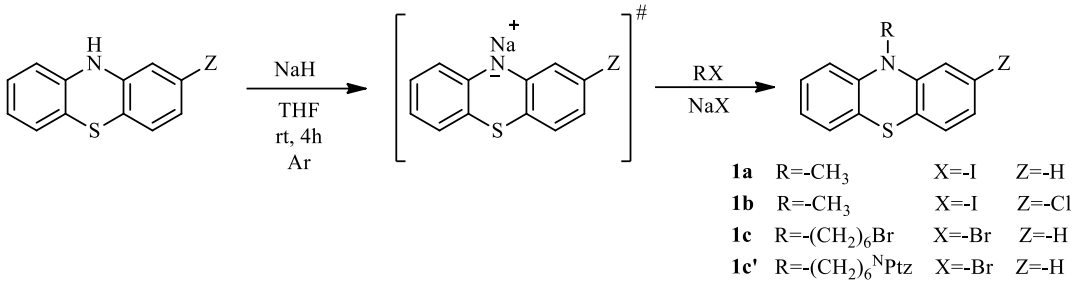

Scheme 2. Synthesis of 10-alkyl-10H-phenothiazine derivatives

The reactions were monitored by thin layer chromatography, the purification of obtained compounds was achieved by recrystallization from ethanol (**1a**, **1b**) and column chromatography (**1c**, **1c'**) with silica, using toluene as eluent. The structures of obtained derivatives were studied by mass spectrometry (where the spectra show some typical fragments for this type of compounds) and NMR spectroscopy methods. The ^{1}H- and ^{13}C-NMRs, recorded in $CDCl_3$, confirm the structure of the alkylated phenothiazines, the corresponding aliphatic and aromatic proton signals were in accordance with literature data.

3.1.2. N-alkyl-10*H*-phenothiazine-carbaldehides

Phenothiazine 3- and 7-carbaldehyde derivatives were successfully obtained by Vilsmeier-Haack reaction, a method proposed by Bodea[123] in 1965 with minor modification: the first step was the formation of electrophilic agent, formed at 0^{o}C, from DMF and $POCl_3$ (obtained an iminium salt, called Vilsmeier formylating agent), which was followed by the addition of corresponding 10alkyl-10*H*-phenothiazine, dissolved in 1,2-dichloroethane and refluxed for 6 hours (*Scheme 3*).

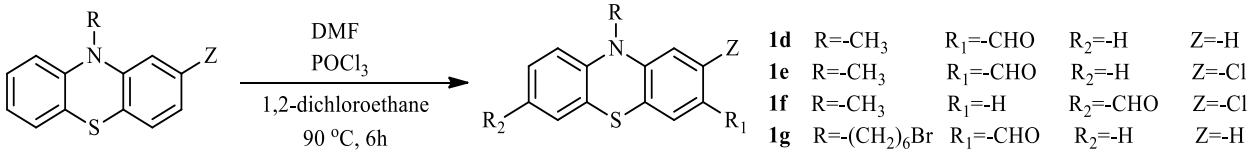

Scheme 3. Synthesis of 10-alkyl-10H-phenothiazine-carbaldehydes

The preparation of unsymmetrically functionalized 7-bromo-10alkyl-10*H*-phenothiazine-3-carbaldehydes was achieved by a method described by Kramer[124], which avoided the halogen exchange, caused by $POCl_3$. Starting from **1d** the bromination reaction with elemental bromine in acidic media results the mono-bromo-N-alkyl-phenothiazine-carbaldehyde derivative in moderate yield.

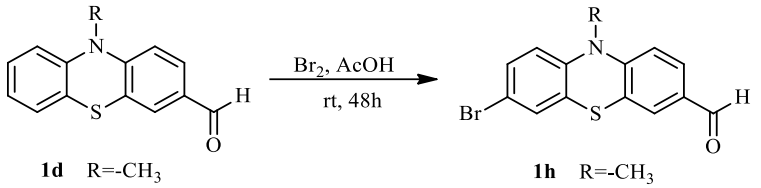

Scheme 4. Synthesis of unsymmetrically functionalized phenothiazines

Purification of synthesized compounds was achieved by silica gel column chromatography, using toluene as eluent. The structure of synthesized compounds was confirmed by ^{1}H-NMR, ^{13}C-NMR and mass spectrometry (MS) methods and showed spectroscopic data in good agreement with those reported in literature. In the ^{1}H-NMR spectra of obtained compounds were identified separately: the corresponding signals of the six different aromatic protons (6.6-7.7 ppm), protons of the alkyl chain (1.3-4 ppm) and formyl protons (9.7-10.3 ppm). In case of **1g**, doublets associated H_1 and H_9 protons appeared overlapped due to their similar chemical shifts (*Figure 10*).

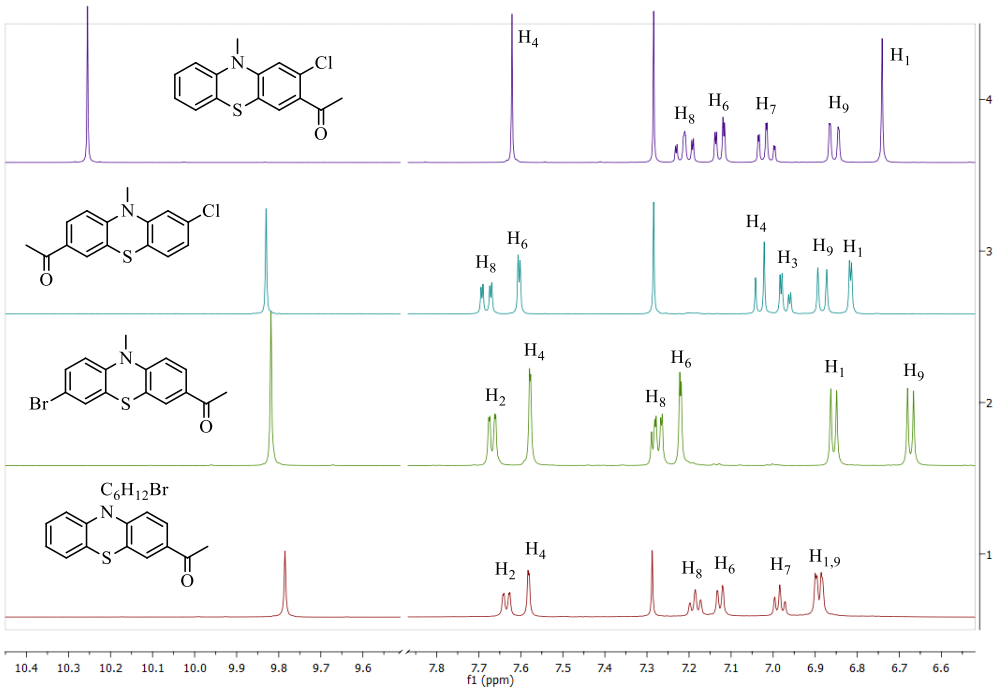

Figure 10. Comparative ^{1}H-NMR spectra of N-alkyl-10H-phenothiazine-carbaldehydes (aromatic part, $CDCl_3$, 400 MHz)

3.1.3. N-alkyl-10*H*-phenothiazine-boronic acids

Phenothiazine-boronic acid derivatives were prepared in standard Suzuki coupling conditions: a mixture of bromo-phenothiazine, bis(pinacolato)diboron and potassium carbonate in

presence of $Pd(PPh_3)_4$ catalyst were heated to reflux for 18 hours[24]. The reactions were monitored by thin layer chromatography (with toluene), the crude compounds were purified by column chromatography and afforded the corresponding boronic ester derivatives as yellowish solid in good yield. The identification of products was achieved by ^{1}H-, ^{13}C, ^{11}B-NMR and mass spectral analysis (MS), the obtained results confirmed the proposed structure of compounds in accordance with literature data.

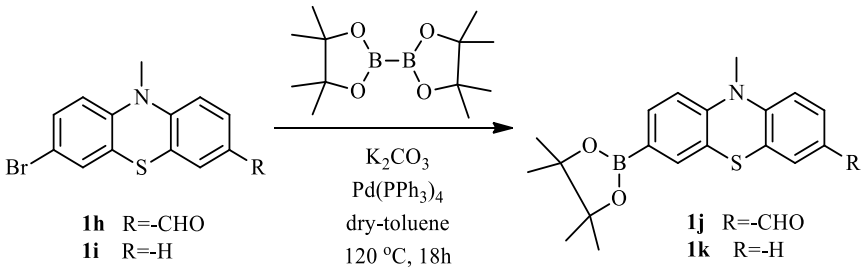

Scheme 5. Synthesis of 10-alkyl-10H-phenothiazine-boronic acid derivatives

3.1.4. Vinyl-phenothiazine derivatives

Based on literature data, the vinyl-phenothiazine derivatives were mostly synthesized by Wittig reaction in presence of methyltriphenylphosphonium iodide in moderate to good yields (28-84%)[125,126]. In our case, for the preparation of vinyl-phenothiazine a new method was used to eliminate the application of triphenyl phosphonium ylide. In first step 10-methyl-10*H*-phenothiazine (**1a**) was treated with H_3PO_4 in acidic media to afforded 3-acetyl-10-methyl-10*H*-phenothiazine (**1d**) in good yield. Then sodium borohydride reduction of obtained acetyl-derivative gave the desired phenothiazine-ethanol compound (**1d'**), which was postfunctionalized in dehydration reaction using copper (II) sulfate anhydrous and hydroquinone (to prevent the polymerization) to generate the 3-vinyl-10-methyl-10*H*-phenothizine (**1m**) as final product. The reactions were monitored by thin layer chromatography and visualized by UV light. In last two reaction steps, the formed compounds were purified by silica gel column chromatography using toluene as eluent.

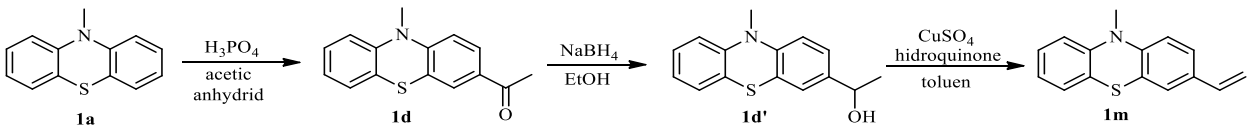

Scheme 6. Synthesis of 3-vinyl-10-methyl-10H-phenothiazine

The structures of phenothiazine derivative were determined on the basis of spectral data (^{1}H-, ^{13}C-NMR and MS). In every case, the characteristic singlet generated by the methyl (N-CH_3) protons appeared around 3.30 ppm in aliphatic part. The corresponding aromatic proton signals were situated between 6.70-7.80 ppm and gave characteristic signals of phenothiazine unit substituted at position 3: doublet for H_1 and H_9, triplet for H_7 and H_8, singlet for H_4 and doublet-doublet for H_2. In addition, in the ^{1}H-NMR spectrum of **1m** displayed two doublets at 5.16 (J=10.8 Hz) and 5.64 (J=17.5 Hz) ppm for *cis* and *trans* protons, respectively a double-doublet at 6.62 ppm which confirmed the presence of vinyl group.

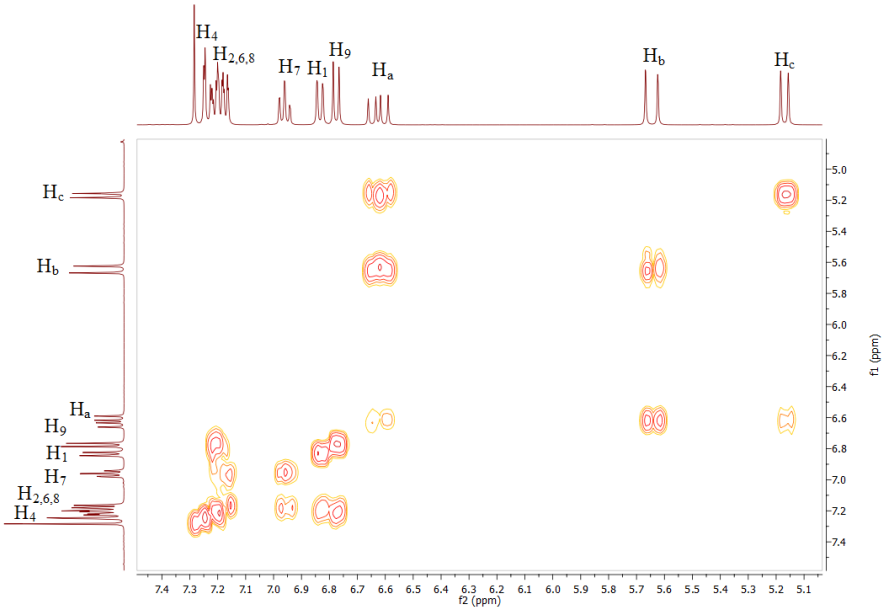

*Figure 11. (^{1}H-^{1}H) COSY spectrum of **1m** (detail, $CDCl_3$, 400 MHz)*

The structure of **1m** was also highlighted with 2D homonuclear (^{1}H-^{1}H COSY) and heteronuclear (^{1}H-^{13}C HMQC) NMR measurements. The ^{1}H-^{1}H COSY spectrum showed the *ortho* coupling of protons H_1 and H_2 (^{3}J=8.0 Hz), and the *meta* coupling of H_2 and H_4 (^{4}J=1.9 Hz) on the first benzene ring. In the case of second ring, we observed the *ortho* coupling between H_6 and H_7 (^{3}J=6.5 Hz), H_8 and H_9 (^{3}J=8.3 Hz), respectively the *meta* coupling of protons H_6 and H_8 (^{4}J=1.4 Hz), H_7 and H_9 (^{4}J=1.0 Hz).

3.1.5. N-alkyl-10*H*-alkynyl-phenothiazine derivatives

The synthesis of terminal alkynyl-phenothiazine was achieved by elimination reaction of alkyl-halides[127]: bromo-phenothiazine aldehyde (**1h**) and trimethylsilylacetylene in alkali media

were heated to reflux under inert atmosphere, in presence of palladium(II) acetate. The work-up and purification procedures afforded the trimethylsilyl-ethynyl-phenothiazine (**1o**) as yellow solid in good yield. Deprotection of trimethylsilyl group with K_2CO_3 gave the desired alkynyl phenothiazine (**1q**).

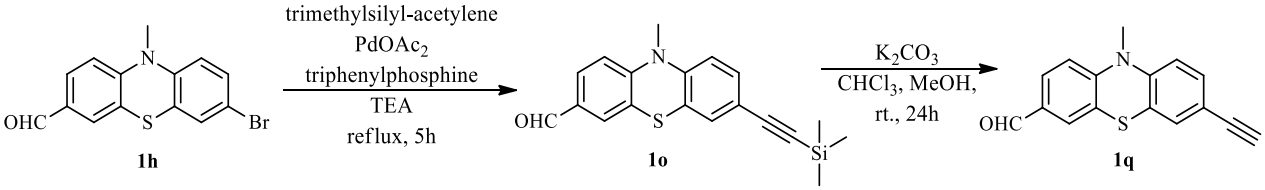

Scheme 7. Synthesis of 7-ethynyl-10-methyl-10H-phenothiazine-3-carbaldehyde

The structure of known phenothiazine derivative was established by NMR and mass spectrometry measurements, the spectroscopic results were in accordance with literature data. The ^{1}H- and ^{13}C-NMR were recorded in $CDCl_3$ at 400 MHz. The corresponding signals of the aromatic protons appeared between 6.76 and 7.68 ppm, the aldehyde proton signal occurred at 9.83 ppm, is strongly deshielded due to the anisotropic field of C and O atoms, while the most shielded ethynyl proton appeared as a singlet at 3.10 ppm. The obtained ethynyl-phenothiazine compound was used as precursor for the synthesis of ethynyl bridge linked phenothiazinyl-phenyl aldehydes.

3.1.6. N-alkyl-*10H*-alkynyl-bridge phenothiazinyl-phenyl aldehydes

The acetylene linked phenothiazine derivatives were prepared by Sonogashira cross-coupling reactions[128]: a mixture of aryl halide and aryl ethynyl derivative in alkali media was heated to reflux in presence of palladium/copper catalytic system, under inert atmosphere.

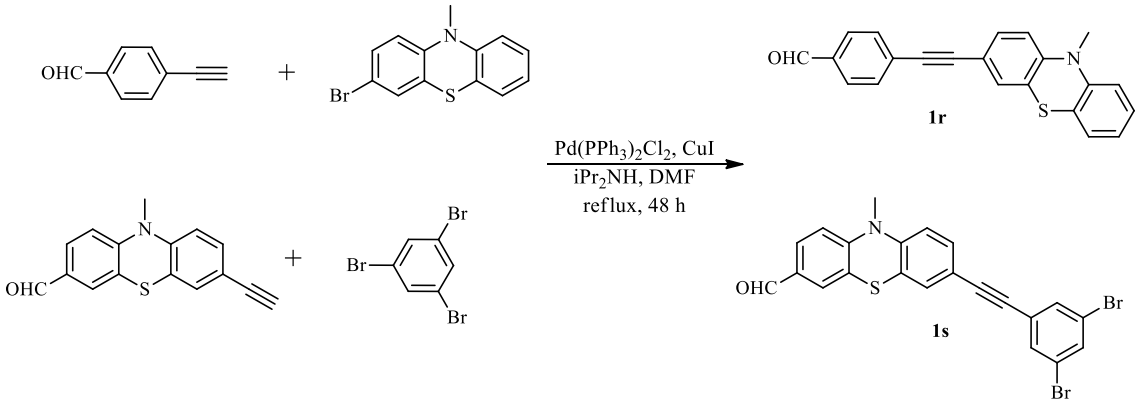

Scheme 8. Synthesis of ethynyl bridge linked phenothiazinyl-phenyl aldehydes

The reactions were monitored by thin layer chromatography, after work-up and purification procedures the products (**1r**, **1s**) were isolated in moderate to good yield. The aim of this procedure was to extend the phenothiazine moiety with aromatic units via ethynyl spacer and remove the steric hindrance between the phenothiazine and the phenyl groups.

The 1D (^{1}H, ^{13}C) and 2D (COSY, HMQC) NMR analysis confirm the proposed structure of desired products. The characteristic singlet generated by the formyl proton appeared at 10.02 ppm, the signals of the seven different aromatic protons occurred between 6.78 and 7.38 ppm, while the symmetrically functionalized benzene unit gave two distinct signals situated at 7.64 ppm (H_b) and 7.88 ppm (H_a), which is the most deshielded aromatic proton, due to the electronic effect of formyl group.

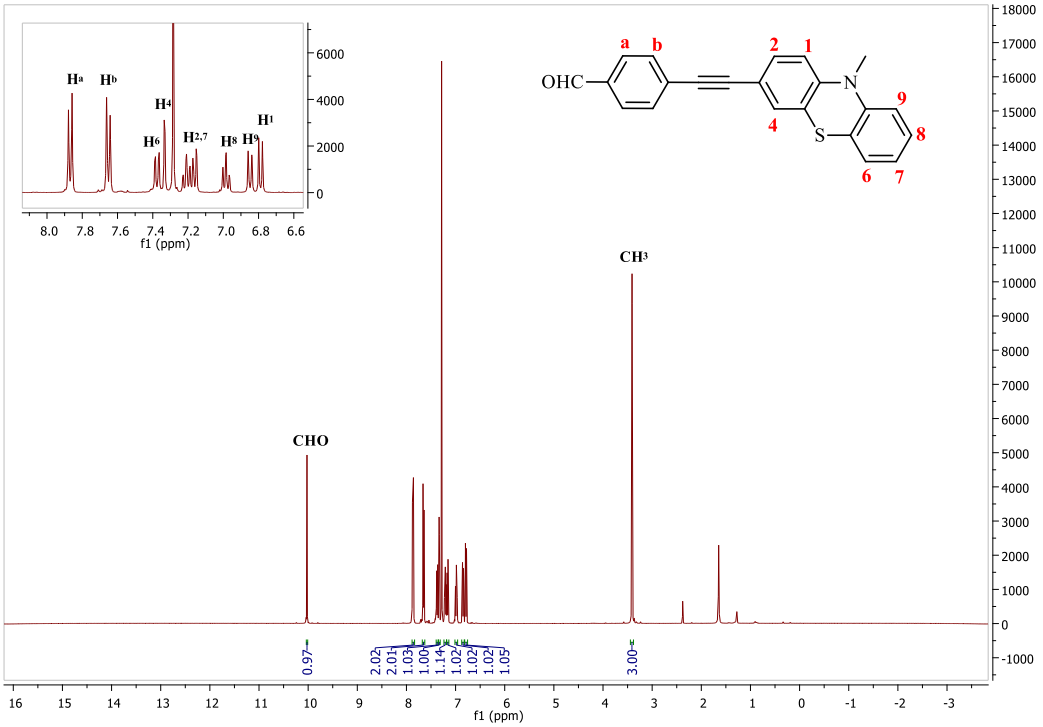

*Figure 12. ^{1}H-NMR spectrum of **1r** compound ($CDCl_3$, 400 MHz)*

3.1.7. Conclusions

In this part of thesis, a series of N-alkyl-10*H*-phenothiazine derivatives were prepared using different synthetic methods. The strategy for the synthesis of phenothiazine precursors includes three reaction steps: first the N-alkylation of heterocyclic nitrogen, followed by the Vilsmeier-Haack formylation of the phenothiazine core and functionalization of N-alkyl- or N-

alkyl-3-formyl-phenothiazine by modified Wittig, Suzuki and Sonogashira cross-coupling reactions.

10-alkyl-10*H*-phenothiazines (**1a**, **1b**, **1c**, **1c'**) and their formyl derivatives (**1d**, **1e**, **1f**, **1g**, **1h**) were successfully obtained in moderate to good yields with carefully selected reaction conditions (substrate, reaction temperature). Then, bromo phenothiazine derivatives were converted to the corresponding phenothiazinyl boronic esters (**1j** and **1k**) through Pd-catalyzed borylation with bis(pinacolato) diboron as boron source. The use of K_2CO_3 as a base and the catalytic amount of $Pd(PPh_3)_4$ worked well in these Suzuki coupling reactions.

For the synthesis of vinyl phenothiazine derivative (**1m**) a modified Wittig reaction was applied favorably. Starting from 10-methyl-10*H*-phenothiazine the desired product was achieved in satisfactory yield, avoiding the application of triphenyl phosphonium ylide. Furthermore, for the design of new triple carbon-carbon bonds between the halogenated phenothiazines and alkynes was realized by Sonogashira coupling reaction. Treatment of bromo-phenotiazine derivative with terminal alkynes in iPr_2NH/DMF in the presence of $PdCl_2(PPh_3)_2$ and CuI furnished the corresponding ethynyl-phenothiazine derivatives (**1o**, **1q**, **1r** and **1s**).

Via these synthetic methods, a series of phenothiazinyl based building blocks were prepared and were accessible for the synthesis and postfunctionalization of new phenothiazinyl-porphyrin derivatives.

3.2. Synthesis and functionalization reactions of *meso*-phenothiazinyl-porphyrins

3.2.1. Free-base MPP derivatives: synthesis, optical properties and protonation study

In this part of thesis, we recommended a suitable synthetic protocol for the preparation of star shaped *meso*-tetraarylporphyrins with various phenothiazine arms. The procedure described by Adler-Longo[54] was adapted to the synthesis of A_4-, A_3B- and A_2B_2-type MPP: mixt condensation reaction of formyl-phenothiazine derivatives with aryl-aldehyde (benzaldehyde or 4-bromo-benzaldehyde) and pyrrole in presence of propionic acid and acetic anhydride. The structures of obtained compounds were assigned based on NMR (1D and 2D) and HRMS spectra. Their optical properties were studied using UV-Vis and fluorescence spectroscopic data. The absorption maxima are located around 420 nm (Soret band) with high molar absorptivities values (ε), while the emission spectra are characterized by low quantum yields (Φ_F), but noticeable Stokes shifts.

Titration for a series of MPP was performed using trifluoroacetic acid in DCM, followed by ^{1}H-NMR measurement. The UV-Vis spectra of generated hyperporphyrins showed large batochromic shifts, especially in the case of Q bands a strong and broad absorption are observed at longer wavelengths. Due to these properties, they are good candidates for potential optoelectronic applications.

3.2.1.1. Synthesis of A_4-, A_3B- and A_2B_2-type *meso*-phenothiazinyl-porphyrins

Stoichiometrically mixed condensation of (hetero)aryl aldehydes with pyrrole were used as a direct preparation of A_4-type *meso*-arylporphyrins (*Scheme 9*). Best yields were obtained in case of *meso*-arylporphyrins (**2a**, **2b**, **2c**), without phenothiazine arms, due to the better solubility properties of starting aldehydes and the steric control induced by the non-planar and bowl-shaped[129] structure of phenothiazine-carbaldehyde.

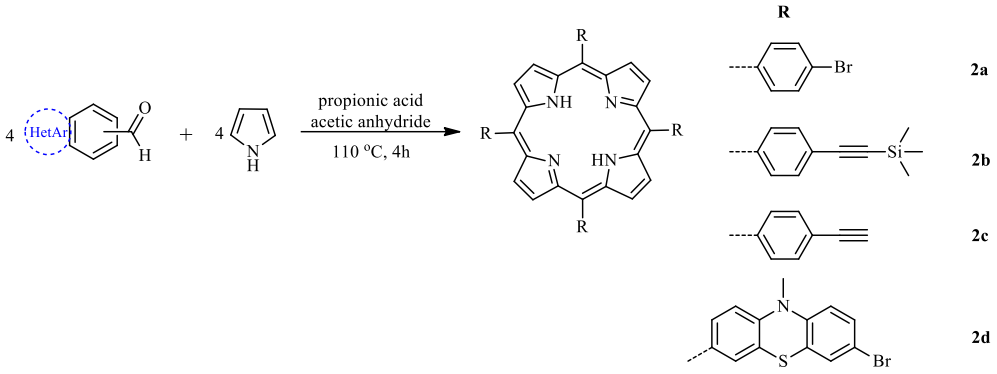

Scheme 9. Adler-Longo synthesis of meso-(hetero)aryl-porphyrins

The advantage of this procedure consists in fact that the target compounds can be used for further synthesis without purification. The structures of known (**2a**, **2b**, **2c**, **2d**) *meso*-arylporphyrins were confirmed by spectroscopic investigations (NMR and HRMS) and corresponded to the proposed structures. The obtained porphyrins are valuable intermediates for additional functionalization reactions.

One-pot synthetic procedure was successfully used for preparation of *meso*-phenothiazinyl-porphyrins containing one or two phenothiazine units directly linked to the porphyrin core. The Adler-Longo mixed condensation reaction of 10-alkyl-10H-phenothiazine-carbaldehydes and benzaldehyde (or 4-bromo-benzaldehyde) with pyrrole afforded a mixture of A_3B- and A_2B_2-type of MPP (*Scheme 10*).

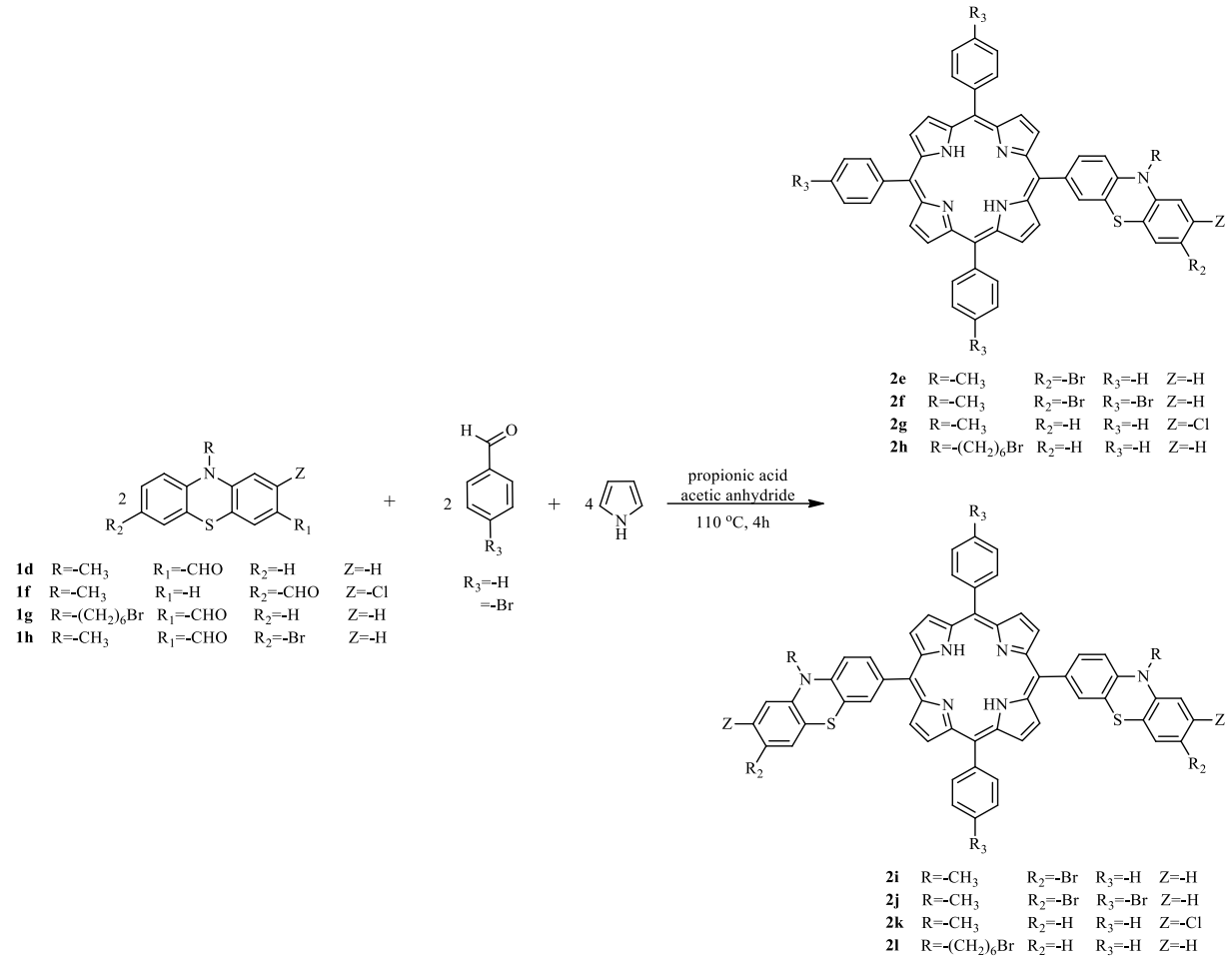

Scheme 10. Adler-Longo synthesis of meso-phenothiazinyl-porphyrins

The purification and separation of obtained porphyrin mixture was achieved by repeated silica gel column chromatography, using dichloromethane-petrol ether as eluent to collect in order A_3B- (**2e**, **2f**, **2g**, **2h**) and A_2B_2-type (**2i**, **2j**, **2k**, **2l**) compounds in 2:1 M ratio.

The structures of novel MPP derivatives were characterized by NMR (^{1}H, ^{13}C, COSY, HMQC, HMBC) and HRMS spectrometry. In the ^{1}H-NMR spectra of free-base MPPs were identified three separate regions: a sharp singlet peak around -2.75 ppm corresponding to the two inner NH protons, followed by the alkyl chain's protons in aliphatic part of spectrum and the aromatic protons of porphyrin and phenothiazine rings at the higher field.

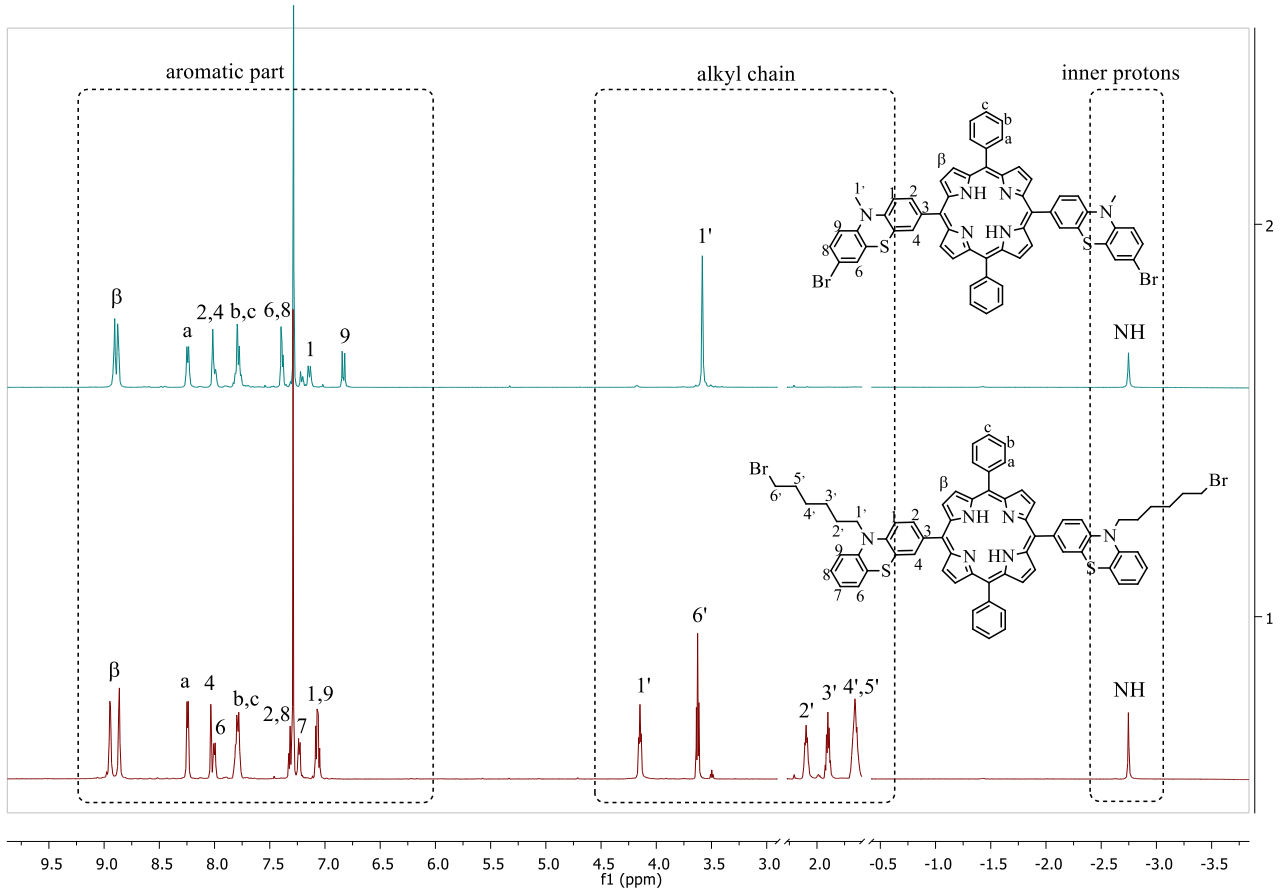

*Figure 13. Comparative ^{1}H-NMR spectra of **2i** and **2l** ($CDCl_3$, 400 MHz)*

In case of **2i** the phenothiazine protecting methyl group signals appeared at 3.4 ppm, while in **2l** spectrum, characteristically the 1' proton is strongly shifted to the downfield region (3.4-4.2 ppm), due to the higher electronegativity of the nitrogen than the bromine atom. The aromatic protons with total integrated intensity were observed between 6.7-8.9 ppm, the position and splitting of these signals were similar to those of starting aldehydes. The most deshielded β-pyrrolic signals appeared as a doublet between 8.6-8.9 ppm with vicinal coupling constant of 4.2 Hz.

Similar one-pot procedures were used for synthesis of (trimethylsilyl)ethynyl- and arylethynyl-porphyrins.

Starting from (trimethylsilyl)ethynyl aldehydes described above (**1o**, **1q**), a series of A_3B-(**2m**, **2n**, **2q**, **2r**) and *trans*-A_2B_2-type porphyrin (**2o**, **2p**, **2s**, **2t**) were prepared in moderate yields (*Scheme 11*).

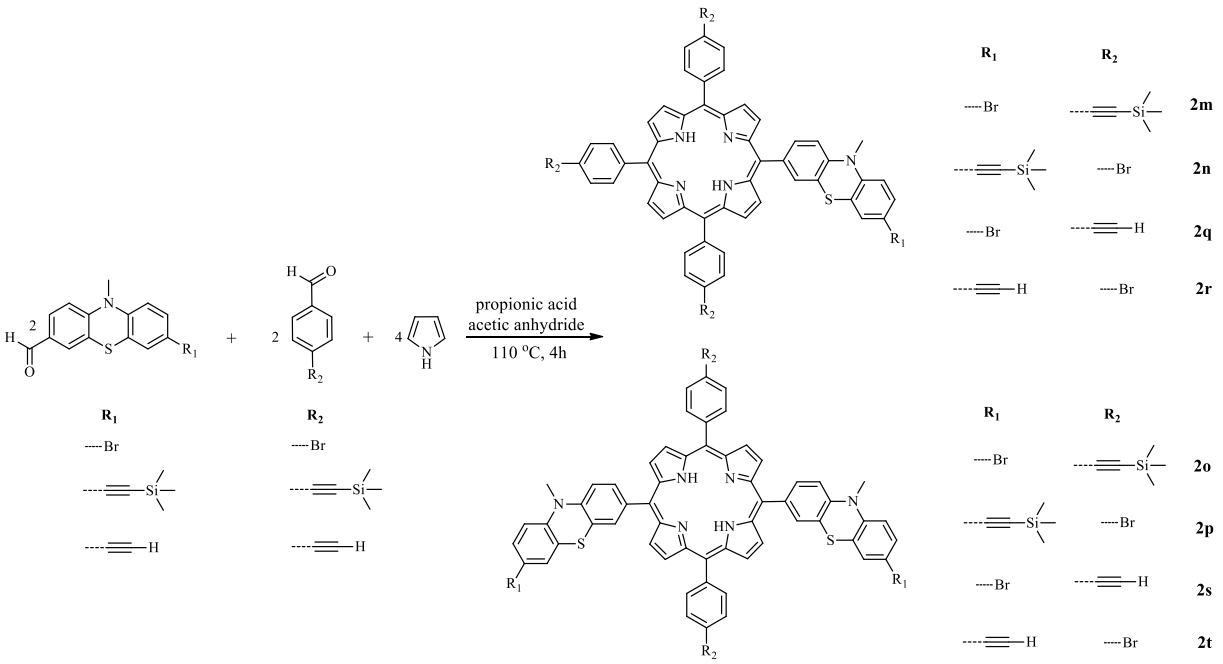

Scheme 11. Synthesis of (trimethylsilyl)ethynyl-porphyrins

After the purification method with column chromatography, the structure of obtained compounds was confirmed by NMR and HRMS analysis, the results of new MPP derivatives were appropriate for the proposed structures. In the ^{1}H-NMR spectrum of **2o** compound, the signals of trimethylsilyl functional group appeared as a sharp singlet at 0.3 ppm, while in case of **2s** this singlet disappeared caused by the deprotection of bulky silyl groups. The chemical shift of formed terminal alkyne's protons was observed at higher field (3.3 ppm), due to the strong shielding effect induced by the magnetic anisotropy of the aromatic rings (*Figure 14*). The ^{13}C-NMR spectra of (trimethylsilyl)ethynyl porphyrins exhibited the aromatic signals in the range δ=112.5-145.8 ppm, internal alkynes signal around 90 and 105 ppm, while terminal alkynes signal around 78 and 83 ppm. The signals of N-protecting methyl groups occurred mostly at 36 ppm and the most upfield shifts exhibited by the trimethylsilyl functional groups appeared between 0.05 and 0.1 ppm.

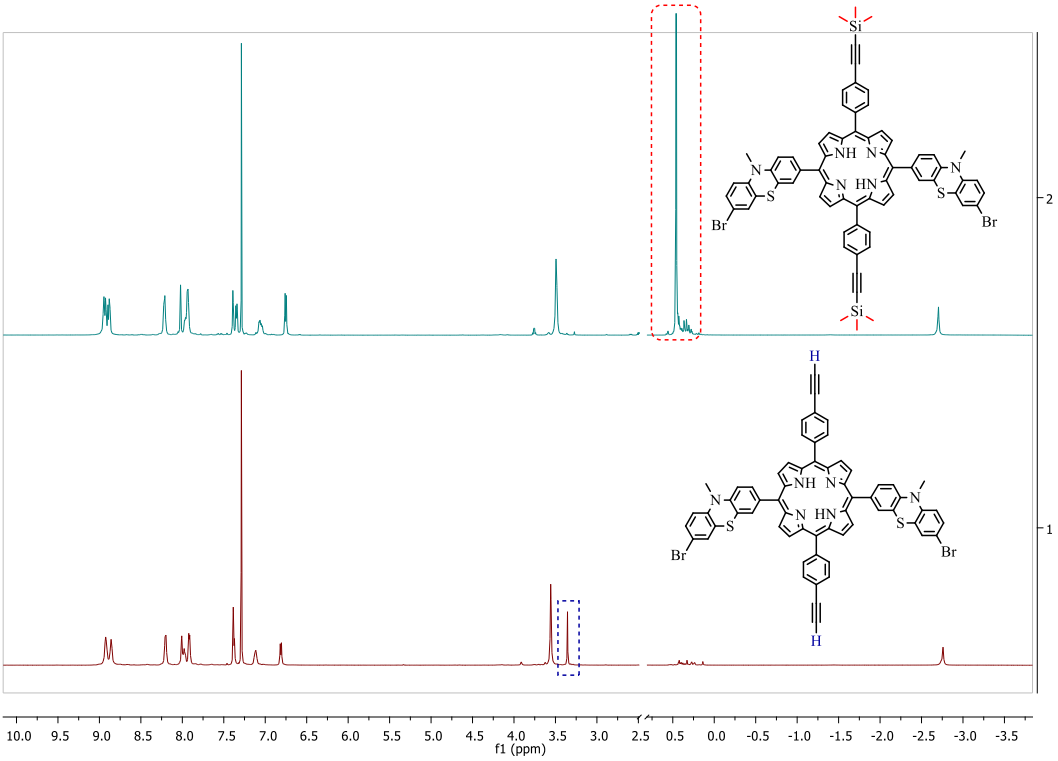

*Figure 14. Comparative ^{1}H-NMR spectra of **2o** and **2s** ($CDCl_3$, 600 MHz)*

In case of arylethynyl-porphyrins (**2v**, **2w, 2x, 2y**), the advantage of starting aldehydes was to extend the phenothiazine moiety with aromatic units via ethynyl spacer (*Scheme 12*).

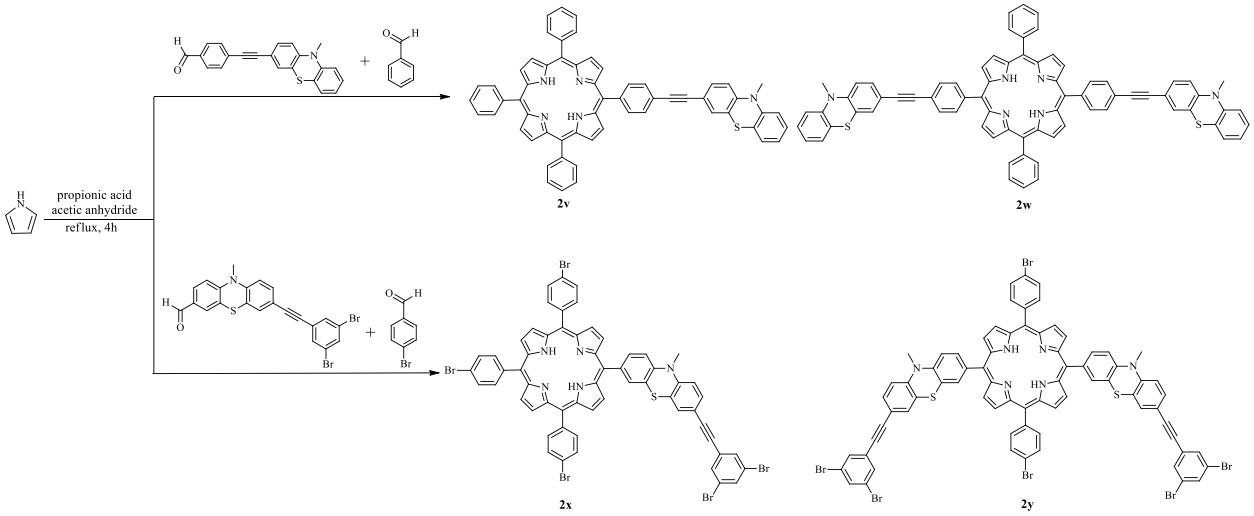

Scheme 12. Synthesis of arylethynyl-porphyrins

Due to the scrambling process, the condensation between heteroaryl aldehydes and pyrrole afforded a mixture of MPP, which was separated by column chromatography. The target compounds were eluted as second (A_3B-type) and third fractions (A_2B_2-type) in 2:1 M ratio.

In the HRMS spectra of each MPP the molecular ion was recorded in high abundance. In case of **2v**, the HRMS study gave a characteristic molecular peak with a correction factor (δ) of 3.6ppm, while the spectrum of **2y** showed a lower correction, 2.4 ppm.

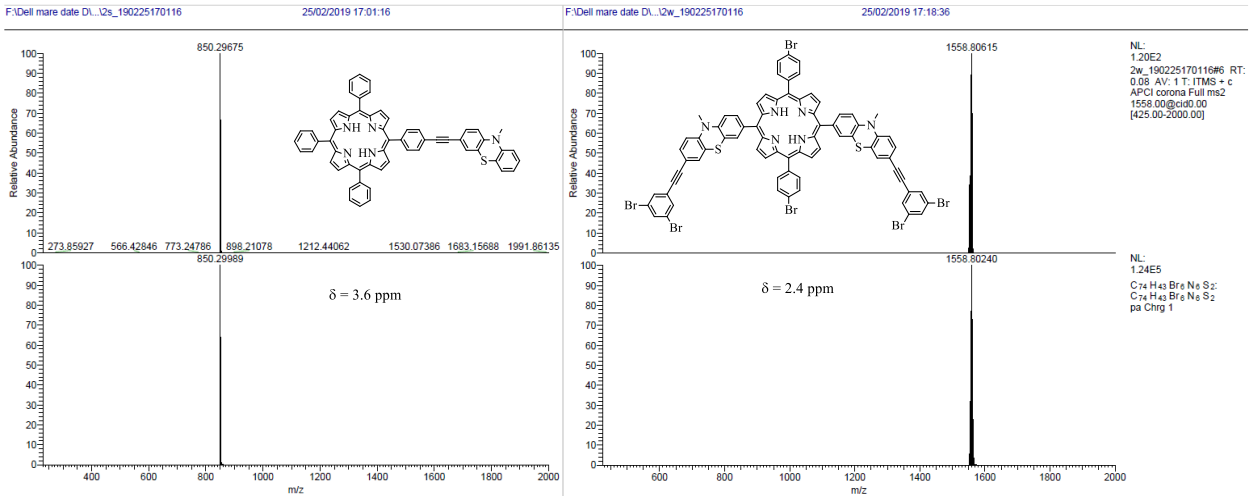

*Figure 15. HRMS (APCI) spectra of compounds **2v** and **2y***

3.2.1.2. Optical properties of MPP derivatives

The photophysical properties for a series of free-base MPP were studied via electronic absorption and emission spectroscopy in both neutral and acidic forms. The introduction of ethynyl bridges between the phenothiazine and aromatic units generated an effective strategy to extend the conjugated π system, which modification results in broadening and noticeable red shifts of the porphyrin absorption bands and the obtained compounds have the ability to emit intense red light with high fluorescence quantum yields.

Absorption and fluorescence studies

In the UV-Vis absorption spectra (*Figure 16a*) of novel MPP derivatives enhanced substituent effect was observed on absorption bands, due to the presence of electron-donating phenothiazine moiety: an intense band around 250 nm created by π-π* transitions in the phenothiazine molecule[130], followed by a strong near-UV Soret band placed at 419-424 nm and followed by four low intensity *etio*-type Q bands situated in the visible spectral region (541-659

nm) (as exemplified in *Figure 16a*). The batochromic shift of the Soret band of all MPP derivatives can be assigned to the increasing number of electron-rich phenothiazine units in the *meso*-position as well as the presence of an intramolecular donor-acceptor molecular framework. A close inspection of the recorded absorption maxima summarized in Table 1 disclosed a minor bathochromic shift of the Soret band (up to 4 nm) upon peripheral functionalization of parent MPP (λ_{abs} 420 nm7) with ethynyl units, best represented by trans-A_2B_2-

type ethynyl-MPP **2o** with peripheral functionalization of the phenyl units with electron donor trimethylsilyl-ethynyl substituents (λ_{abs} 424 nm). Very similar absorption spectrum was recorded upon extending the TPP/MPP derivatives via ethynylene bridges with electron-rich phenothiazine (**2v**, **2w**) or dibromophenylene auxochrome units (**2x**, **2y**). These spectral features signify that the UV-Vis absorption spectra were create mainly by the porphyrin chromophore system, the substituents participating with feeble electronic/steric auxochrome effects. In case of A_3B-type porphyrins higher molar absorptivity were presented in compared to the A_2B_2-types, owing to the less symmetrical structure of compounds, which were advantageous properties for broadening and red-shifting the absorption bands of porphyrin dyes[131].

Table 1. Optical properties of ethynyl-MPP derivatives

Cpd	**λ_{abs} [nm]**						**λ_{em} [nm]**	**Stokes shift [cm^{-1}]**	**Φ_F**[b]
	Ptz	**Soret**[a] **ε [mol^{-1} cm^{-1}]**	**Q_4**	**Q_3**	**Q_2**	**Q_1**			
2m	251	422 (*239167*)	519	556	593	650	658	8499	0.23
2n	252	419 (*172178)*	518	555	591	649	655	8485	0.21
2o	252	424 (*165464*)	520	558	594	651	659	8410	0.21
2p	253	421 (*79531*)	520	557	591	651	658	8443	0.20
2q	252	421 (*283687*)	518	554	591	651	659	8691	0.22
2r	252	420 (*248390*)	519	553	589	648	655	8542	0.21
2s	252	423 (*189598*)	520	559	590	650	658	8555	0.21

2t	252	421 (*111910*)	519	556	591	650	657	8532	0.20
2v	252	420 (*95878*)	514	553	591	648	651	8448	0.23
2w	252	422 (*173379*)	518	554	591	649	656	8452	0.25
2x	253	419 (*184003*)	517	555	592	649	655	8599	0.21
2y	251	421 (*173811)*	519	557	593	651	654	8462	0.11

a-employed for excitation in fluorescence experiments, *b*-quantum yields against TPP standard

Upon excitation with Soret band maxima wavelength, each porphyrin derivative showed red-orange daylight fluorescence in CH_2Cl_2 solution, with large Stokes shift (8410-8691 cm^{-1}) and detectable quantum yields (Φ_F) between 0.11-0.25, pointing them as good candidates for red-emitting materials. The Φ_F values of compounds were calculated against *meso*-tetraphenylporphyrin (TPP) as standard (comparative method of Williams[132]).

The functionalization reaction of the *meso* positions of the phenothiazinyl-porphyrin with ethynyl groups resulted in a remarkable bathochromic shift of the fluorescence peak maxima and stronger fluorescence quantum yields (for exemple, 5,15- bis(arylethynyl)-10,20-diphenyl-porphyrine λ_{em} = 695 nm, λ_{fl} = 0.20[128]). In the case of the newly synthesized compounds, by connecting the TPP system via ethynylene bridges with phenothiazine units, the position of the emission maxima appeared similar to TPP but the fluorescence quantum yield's value became substantially higher (e.g., for **2w** λ_{em} = 656 nm, λ_{fl} > 0.25), situated among the highest values observed for porphyrin derivatives.

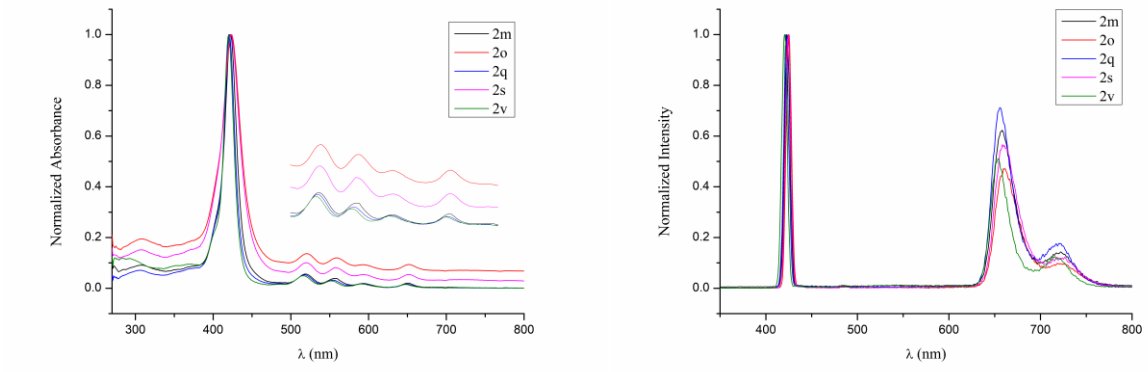

*Figure 16. Normalized absorbance (a.), excitation and emission (b.) spectra of **2m**, **2o**, **2q**, **2s** and **2v** (10^{-5} M and 10^{-6} M in CH_2Cl_2)*

Protonation studies

Porphyrin diacids may be achieved by protonation of the pyrrolic nitrogen atoms and have shown a strong and broad absorption at longer wavelengths relative to the neutral derivatives[133,134,135,136]. Such molecules, also called *hyperporphyrins*[137], cannot be described by Gouterman four-orbital model, due to the implication of additional orbitals leading to charge transfer processes between the donor/acceptor atom and the porphyrin core[138]. These additional orbitals may originate from a central metal in a metalloporphyrin, called *metal-based hyperporphyrins*[139] or from peripheral substituents in case of *acid/base induced hyperporphyrins*[140]. In the latter case, the higher coplanarity of the corresponding substituents, caused by the four N-H bonds of the interior of the ring, significantly extend the already noticeable spectroscopy of porphyrins, along with the broadening and red-shifting of the Soret and Q bands[141].

To the best of our knowledge, there is no report about the acidification study of *meso*-phenothiazinyl-porphyrins.

The potential changes of the photophysical properties of the newly synthesized ethynyl-MPP derivatives in the presence of strong acids were investigated. The protonation study of MPP derivatives was realized in CH_2Cl_2 solution using trifluoroacetic acid (TFA) as the titrating agent. Upon stepwise addition of TFA the MPP macrocycles allowed for gain of two protons on the inner nitrogens to establish a dication (H_2MPP^{2+}) and increased the symmetry of porphyrin core (from D_{2h} to D_{4h} symmetry).

The hypothetical structures of obtained compounds were determined on the basis of ^{1}H-NMR spectral data. In the NMR tube the porphyrins were titrated by 10μl TFA in deuterated $CHCl_3$ with shaking. The study showed that the addition of acid caused the inner NH protons to be chemically shifted downfield during the formation of *hyperporphyrin*, while the pyrrolic *β*-hydrogens were found to move upfield and appeared as a broad singlet around 8.58 ppm. The proton signals of peripheral substituents were observed at higher chemical shifts, moving it to the upfield region (*Figure 17*). These modifications were attributed to the reduced ring current effects, which occurred from geometric distortion of the porphyrin core.

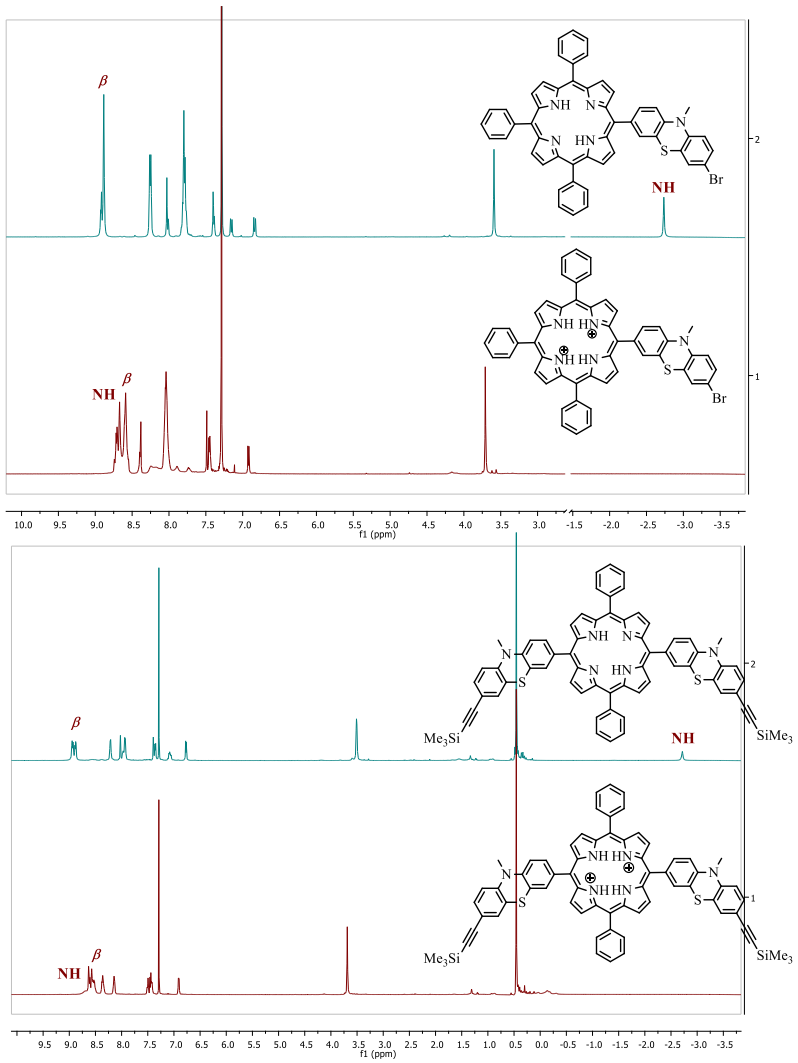

*Figure 17. ^{1}H-NMR spectra of compounds **2e** and **2p** – neutral and acidic form – ($CDCl_3$ + 10μl TFA, 600 MHz)*

The photophysical properties of obtained *hyperporphyrins* were investigated by direct titration with TFA in diluted CH_2Cl_2 solution. In all case a distinct color change from brown to green were observed. As exemplified in Figure 20, showing the modifications recorded in the UV-Vis spectra of the free-bases A_3B-type **2m** with peripheral ethynyl functionalization (*Figure 20a*) and A_2B_2-typeTPP-ethynyl-phenothazine conjugate **2w** (*Figure 20b*), respectively, upon protonation with increasing amounts of TFA (from 10µl up to 100µl), the Soret band appeared more intense and red-shifted with 19 nm with the occurrence of an isosbestic point, while the position of the red hyperporphyrin absorbance situated above 680 nm appeared influenced by the degree of protonation.

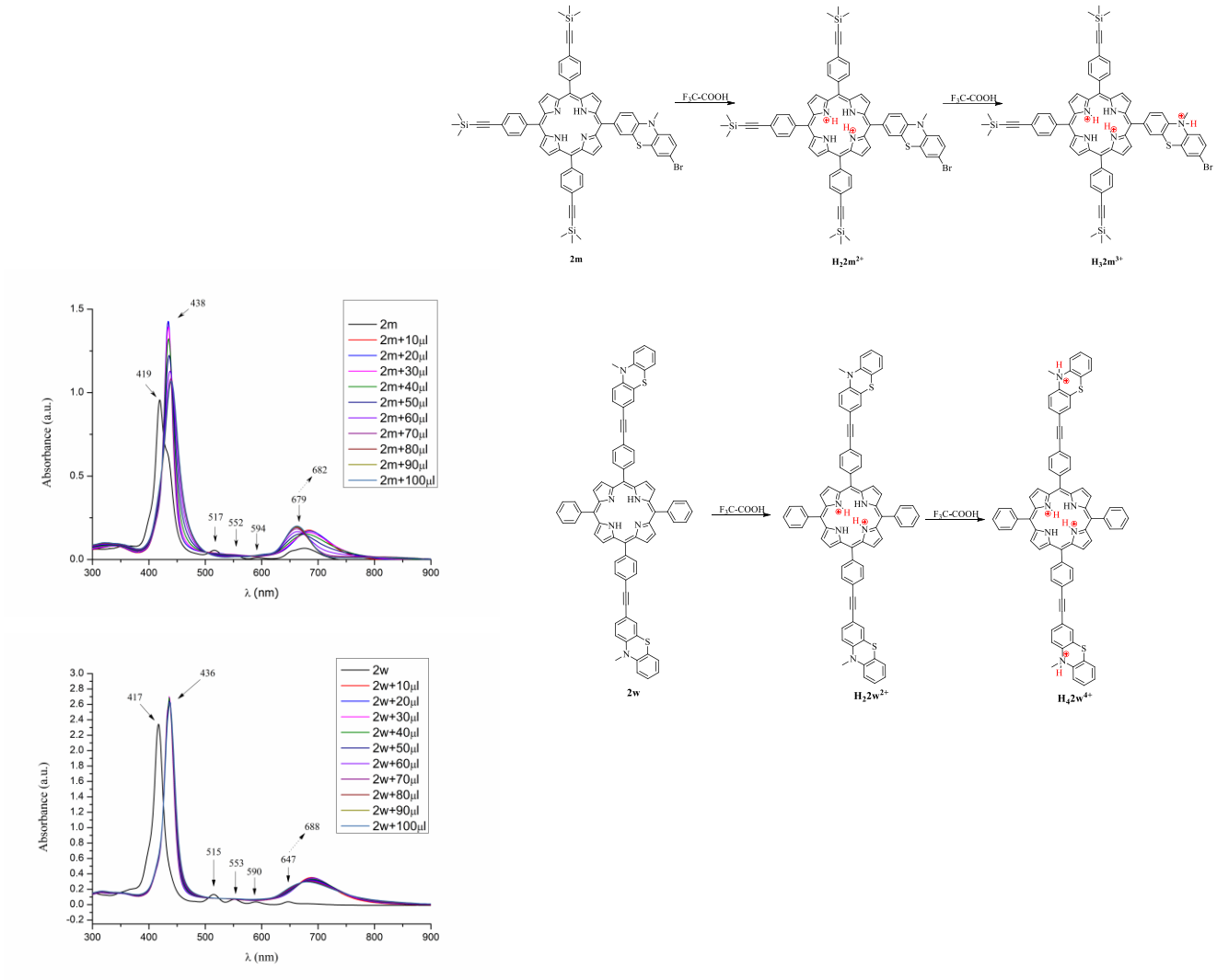

*Figure 18. UV-Vis spectral changes following the addition of 10µl TFA for ethynyl-MPP (10^{-5}M in DCM): a) protonation of **2m**, b) protonation of **2w***

We concluded that addition of 10µl TFA ensured the protonation at the porphyrin core and facilitated the formation of dications $\mathbf{H_2 2m^{2+}}$ (λ_{max}=682nm) and $\mathbf{H_2 2w^{2+}}$ (λ_{max}=688nm) respectively, characterized by a D-A charge transfer between the donor phenothiazine peripheral unit(s) and the acceptor protonated porphyrin core. Further addition of more than 30µl TFA produced a considerable hypsochromic shift of the red absorption band, owing to the effect of the protonation at the nitrogen atom in the phenothiazine unit, which suppressed the electron donor effect of the phenothiazine moiety in $\mathbf{H_3 2m^{3+}}$ (λ_{max}=679nm) and $\mathbf{H_4 2w^{4+}}$ (λ_{max}=649 nm), respectively. This assumption nominates the phenothiazine as a weaker base in comparison to porphyrin.

Figure 21 demonstrated the hyperporphyrin spectra of **H_2TPP^{2+}** and **H_2MPP^{2+}** obtained from TPP and A_3B-type porphyrins **2m, 2g, 2v, 2x** respectively, upon protonation with TFA in CH_2Cl_2 solution. A comparative study of the position of the Soret and Q_4 absorption bands presented in the spectra of the free bases **2m**, **2g**, **2v**, **2x** with those of the corresponding protonated species indicate batochromic shifts of the Soret band (19-26 nm) and significant red shifts of the corresponding Q band (151-176 nm) as a result of the core protonation of the porphyrin, according to the literature data mentioning these specific electronic characteristics upon protonation of TPP and porphyrin functionalized in *meso* positions with ethynyl linkages[140].

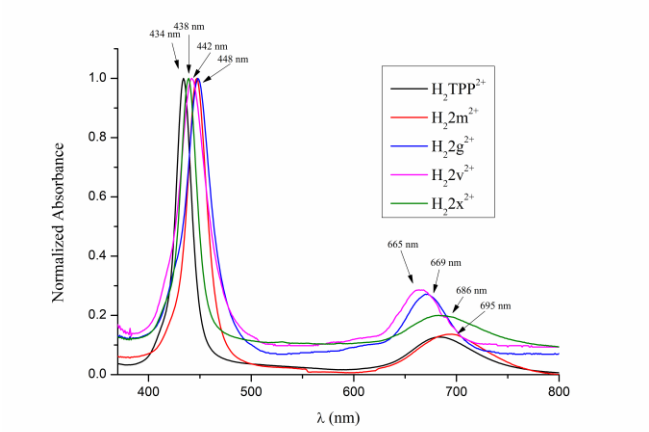

Figure 19. UV-Vis spectral changes following protonation of ethynyl-MPP with 10µL TFA

Almost superimposed Soret bands are observable for similar **$H_2$2m^{2+}**and **$H_2$2g^{2+}** (448 nm) but the long wave maxima showed a 32 nm bathochromic shift for **$H_2$2m^{2+}** containing the electron donor trimethylsilyl substituents. A bathochromic shift of the Soret band was observed for the protonated TPP-ethynyl-phenothiazine conjugate (**$H_2$2v^{2+})** as compared to **H_2TPP**$^{2+}$, indicative of an elongation of the conjugated π-electron system by the electron donor phenothiazine unit. The extension of the conjugated π-electron system of the pending phenothiazine substituent did not generate notable modifications in the absorption spectrum of **$H_2$2x^{2+}**as compared to **H_2TPP^{2+}**.

The fluorescence emission spectra of **H_2MPP^{2+}** derivatives described a red-shifted and broadened emission bands with reduced intensity (*Figure 22a*), except for the case of **2q** (*Figure 22b*) which afforded a clear evidence of efficient energy transfer processes by peripheral substitution with ethynyl groups.

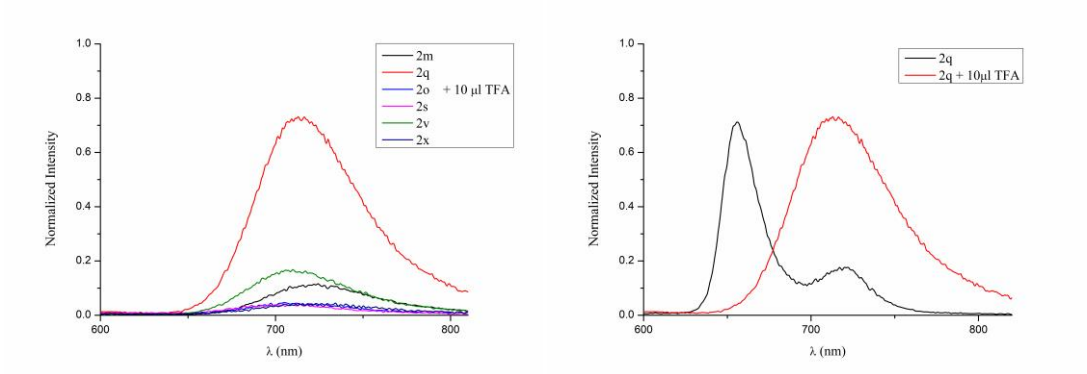

*Figure 20. Fluorescence emission spectra of protonated species a) H_2MPP^{2+}; b) and free base versus protonated **2q** (10^{-6} M in DCM)*

Due to the structural distortion produced upon protonation, hyperporphyrins significantly extend the already beneficial spectroscopic properties of porphyrins and may open new perspectives for further application in optoelectronics.

3.2.2. Metallocomplexes of MPP derivatives: synthesis, optical properties and structural characterizations

The metal insertion into the central cavity of MPP macrocyclic systems was achieved by Adler two-step methods[67]. Thus, metallo-MPP derivatives were prepared by the treatment of previously presented free-base *meso*-phenothiazinyl-porphyrins with the corresponding bivalent metal (Zn, Pd, Ni, Cu) acetate in N,N-dimethylformamide solution at high temperature (*Scheme 13*). The A_3B- and A_2B_2-type metallo-MPPs were obtained in good yields (80-95%) and were further characterized by HRMS and NMR spectroscopic techniques. In case of zinc-, palladium- and nickel-complexes the ^{1}H-NMR analysis confirmed the structures of target metallo-MPPs by disappearance of the inner NH protons signal situated around -2.8 ppm. In the aliphatic and aromatic part, the nature and position of peaks didn't change significantly as compared to the corresponding free-base MPPs.

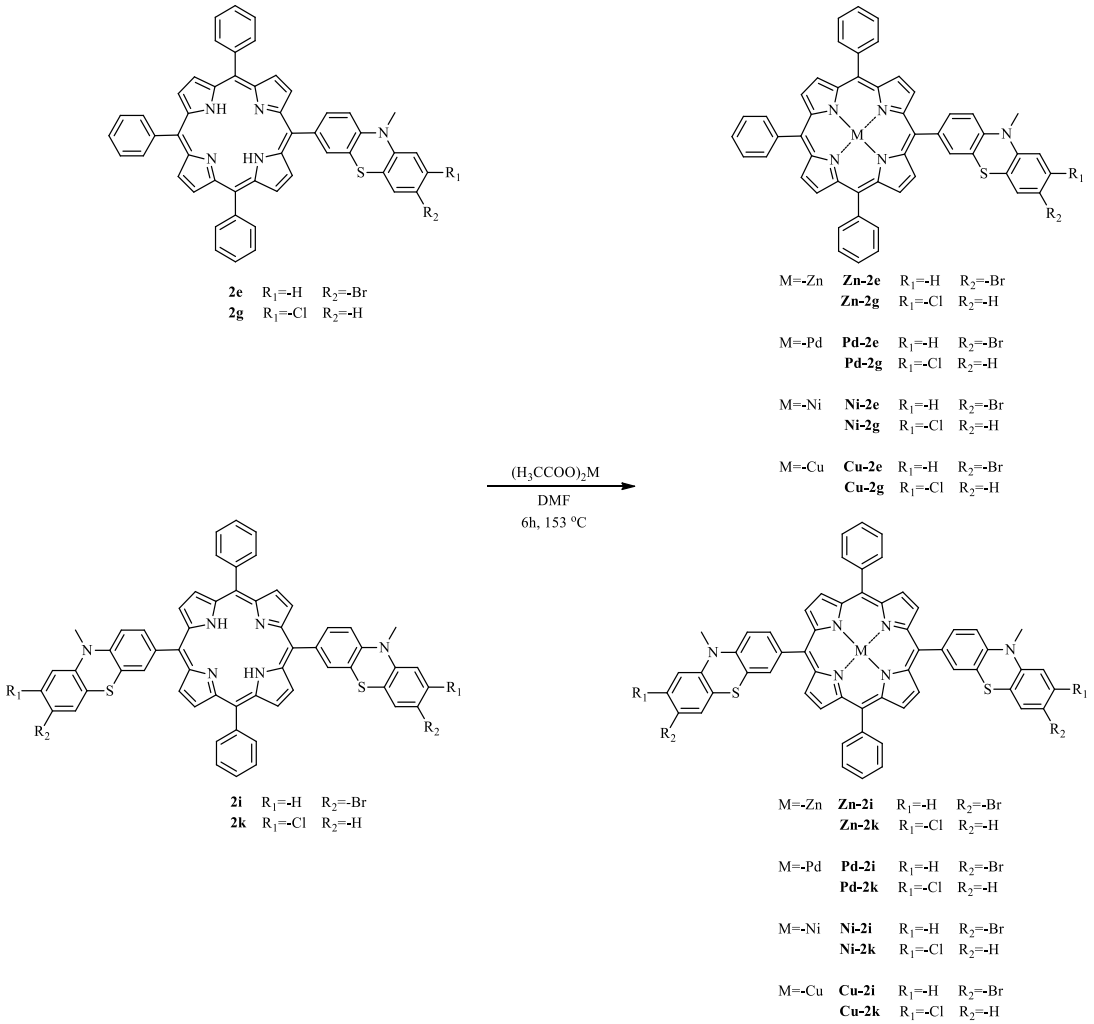

Scheme 13. Synthesis of A_3B- and A_2B_2-type metallo-MPP derivatives

Optical properties of metallo-MPP

The electronic spectra of obtained metallo-MPP derivatives, recorded in DCM solution, included an intense Soret band in the near UV region and a reduced number (one or two) of Q bands. In case of *regular* metalloporphyrins (**Zn-2e**, **Zn-2g**, **Zn-2i**, **Zn-2k**, **Pd-2e**, **Pd-2g**, **Pd-2i**, **Pd-2k**), a very little effect on the porphyrin π to π* energy gap was observed, while the *hypsoporphyrins* containing Ni(II) and Cu(II) ions (**Ni-2e**, **Ni-2g**, **Ni-2i**, **Ni-2k**, **Cu-2e**, **Cu-2g**, **Cu-2i**, **Cu-2k**) showed a remarkable metal *d*π to π* orbital interaction characterized by a small hypsochromic (blue) shift, due to the decreased electron density on the porphyrin core.

The UV-Vis absorption spectra of metallo-MPPs presented slightly red shifted absorption maxima for A_2B_2-type complexes, due to the two phenothiazine substituents directly attached to the porphyrin core. Furthermore, the absorption spectra of **M-2g** derivatives showed a batochromic

shift of the Q bands for **Zn-2g**, while a broadened Soret-and a more intense Q band can be observed for **Pd-2g**, caused by the nature of the metal center. (*Figure 21*).

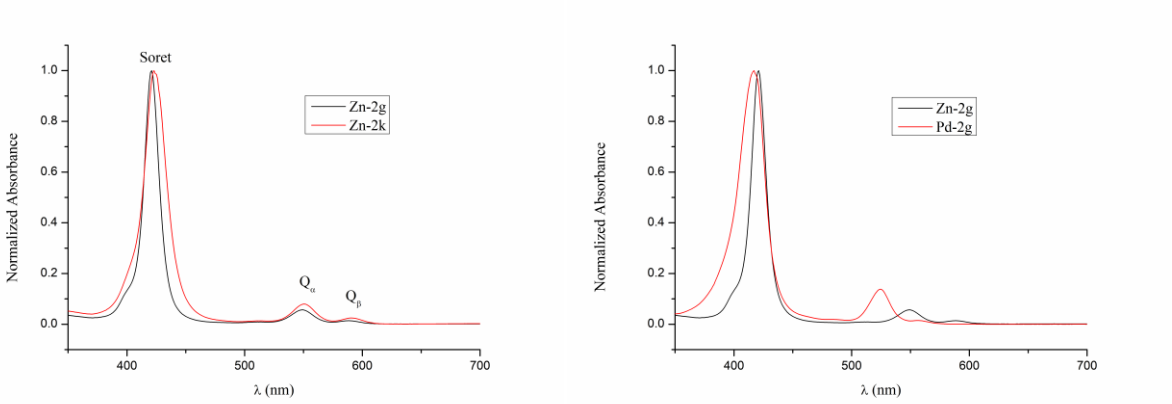

Figure 21. Normalized absorbance spectra of A_3B- and A_2B_2-type metallo-MPPs (a.) with different metal ions (b.) (10^{-5} M in CH_2Cl_2)

Similar to the corresponding free-base porphyrins, the protonation studies of metallo-MPP derivatives were realized in solution using trifluoroacetic acid (TFA) as the titrating agent. Due to the stepwise addition of TFA to a dichloromethane solution of metallo-MPPs a high intensity and broadened Soret band was observed, especially in case of A_2B_2-type compounds. The Q band region changed to one major peak noticed around 700 nm, with the presence of one isosbestic point.

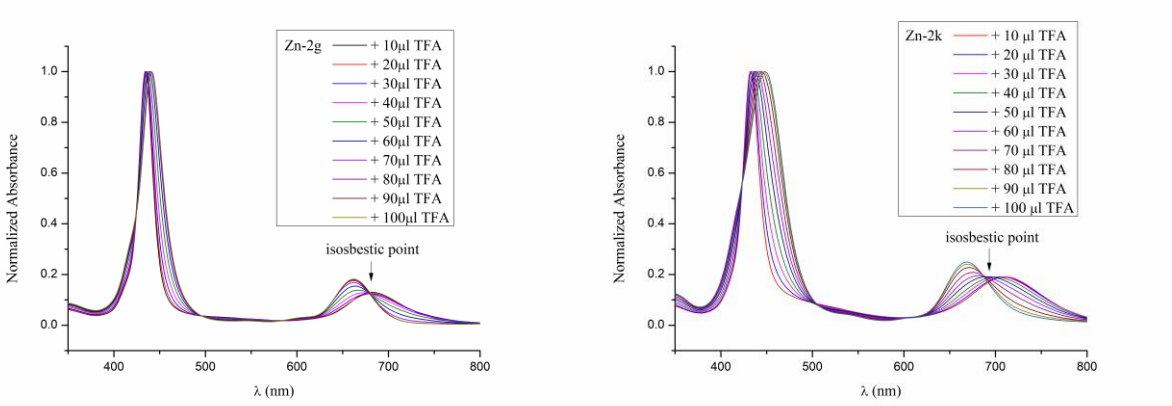

Figure 22. UV-Vis titration of A_3B- and A_2B_2-type metallo-MPPs (10^{-5} M in CH_2Cl_2)

Owing to an increase in symmetry (from D_{2h} to D_{4h}), the batochromic shift of the Soret band were more significant (28 nm) in case of free-base porphyrins, namely the structure of metallo-MPPs were highly symmetrical in neutral form. In addition, in the Q band region of

metallo-MPPs a remarkable spectral change appeared (more than 100 nm red shift), due to the better charge-transfer transition between the phenothiazinyl substituents and the porphyrin ring.

Table 2. Comparative UV-Vis absorption data for free-base and metallo-MPPs

Cpd	Soret band			Q band					
	λ_{max} [nm]		Shift* [nm]	λ_{max} [nm]					Shift* [nm]
	Neutral form	Cationic form		Neutral form				Cationic form	
2g	419	440	**21**	515	552	594	654	684	30
2k	423	451	**28**	517	554	594	654	676	22
Zn-2g	421	435	14	550		588		683	**95**
Zn-2k	423	433	10	550		591		710	**119**

* observed batochromic shift upon protonation of free-base and metallo-MPPs

Under appropriate conditions, the free-base- and metallo-MPPs demonstrated "hyperporphyrin" spectra with perturbed and beneficial photophysical properties relative to the neutral forms. Upon protonation, both series of *meso*-phenothiazinyl-porphyrins presented substantial batochromic shift to an extent dependent on the peripheral substituents, allowing for the study of intensified light-harvesting properties in the red zone of the spectrum.

3.2.3. Cross-coupling products of MPP derivatives

3.2.3.1. Suzuki-Miyaura cross-coupling products

The synthesis of *meso*- and *β*-cross-coupling products were carried out using A_4-, A_3B- and A_2B_2-type bromoporphyrins and (hetero)aryl boronic acid derivatives.

Synthetic procedures

The preparation of A_4-type cross-coupling compounds (**3a**, **3b**, **3c**) were realized under standard Suzuki-Miyaura conditions using $Pd(PPh_3)_2Cl_2$and K_2CO_3 as catalyst and base in DME-H_2O solvent mixture. Starting from 5,10,15,20-tetrakis-(4-bromophenyl)-*21,23H*-porphyrinand boronic acid derivatives, such as 4-formylphenylboronic acid, 4-(9*H*-carbazol-9-yl)phenyl)boronic acid and 10-methyl-7-(4,4,5,5-tetramethyl-1,3,2-dioxaborolan-2-yl)-10*H*-phenothiazine-3-carbaldehyde,the desired star-shaped cross-coupling products were formed in

good yields (~60%), owing to the sterically unhindered *meso*-positions. The applied tetrabrominated porphyrin was obtained by Adler-Longo method, which involves the stoichiometrically condensation of 4-bromo-benzaldehyde and pyrrole in presence of propionic acid at high temperature.

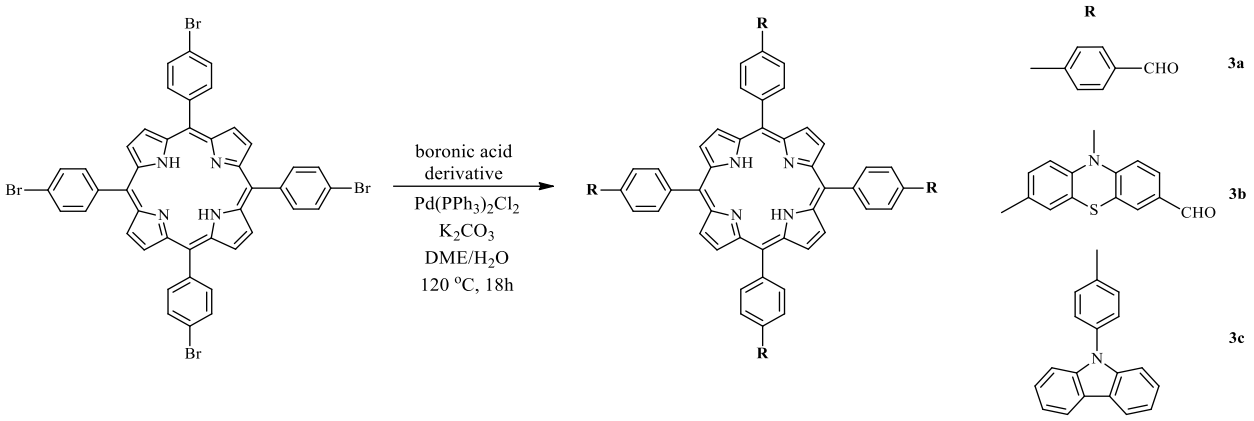

Scheme 14. Suzuki cross-coupling reaction of A_4-type porphyrins

Under appropriate conditions, the Suzuki-Miyaura reaction of free-base- and metallo-*meso*-phenothiazinyl-porphyrins was also studied. Cross-coupling of A_3B-type MPPs (**2e**, **Zn-2e**) and (hetero)aryl boronic acid derivatives was carried out in a mixture of DME and H_2O in the presence of catalytic amount of $Pd(PPh_3)_2Cl_2$ and 1.5 eq. of K_2CO_3 at 120 °C under inert atmosphere to give the target products in moderate to good yield (40-70%).The application of metallo-MPPs as coupling partners was a successful strategy, which increased the reaction yield (66-70%) and simplified the purification method.

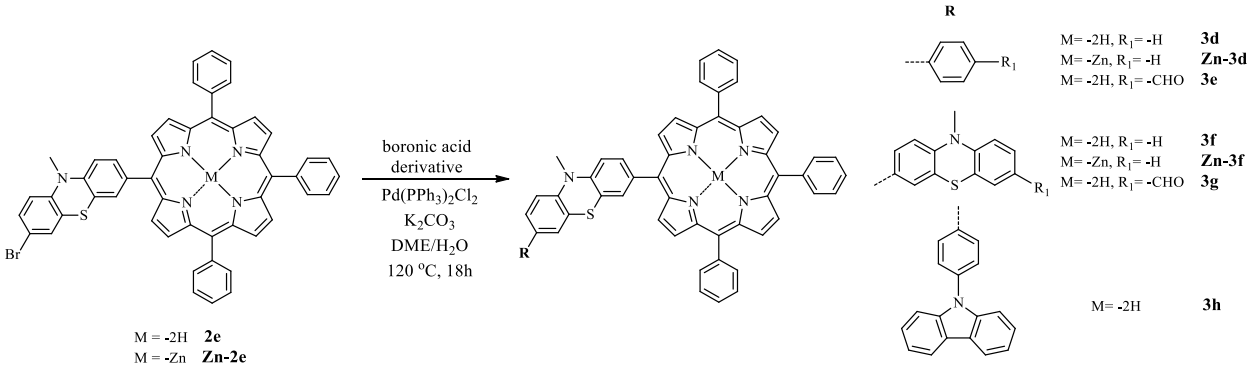

Scheme 15. Suzuki cross-coupling reaction of A_3B-type meso-phenothiazinyl-porphyrins

Using the same conditions A_2B_2-type *trans*-MPP cross-coupling products were also prepared via palladium-mediated Suzuki-Miyaura reaction, using free-base dibrominated-MPP

(**2i**) and (hetero)aryl boronic acid derivatives as coupling partners. The introduction of formyl functionalities (**3i**, **3j**) allows the bidirectional connection of other substituents to construct complex macrocyclic structure.

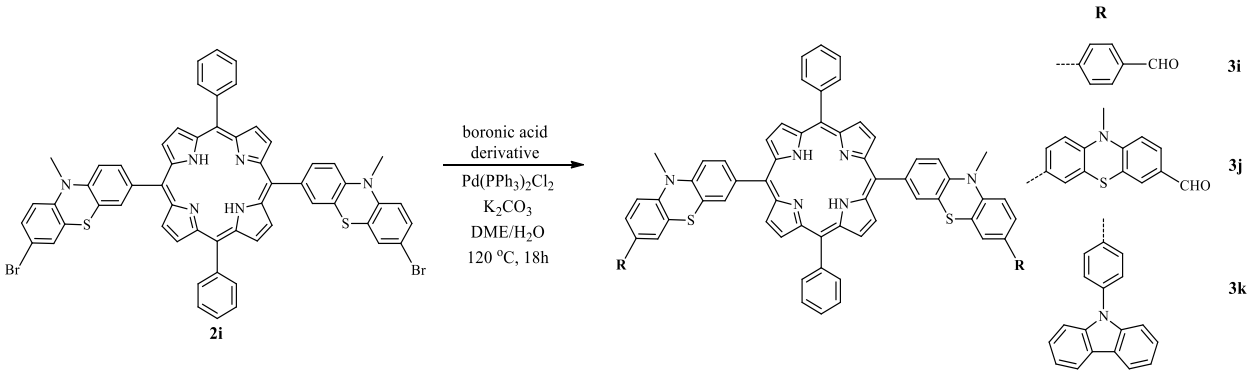

Scheme 16. Suzuki cross-coupling reaction of A_2B_2-type meso-phenothiazinyl-porphyrins

This process leads to functionalized *meso*-phenothiazinyl-porphyrins in high yield, under mild conditions.

The compatibility of the porphyrin skeleton functionality was also investigated using *β*-substituted porphyrins. The reaction between 2-bromo-5,10,15,20-(tetraphenyl)-21,23*H*-porphyrin and phenyl/phenothiazinyl-boronic acids, under standard Suzuki-Miyaura coupling conditions (Pd catalyst, base) afforded the desired compounds (**3l**, **3m**, **3n**) in satisfactory yield. The synthetic route for the (hetero)aryl-functionalized *β*-porphyrins are presented in *Scheme 17*.

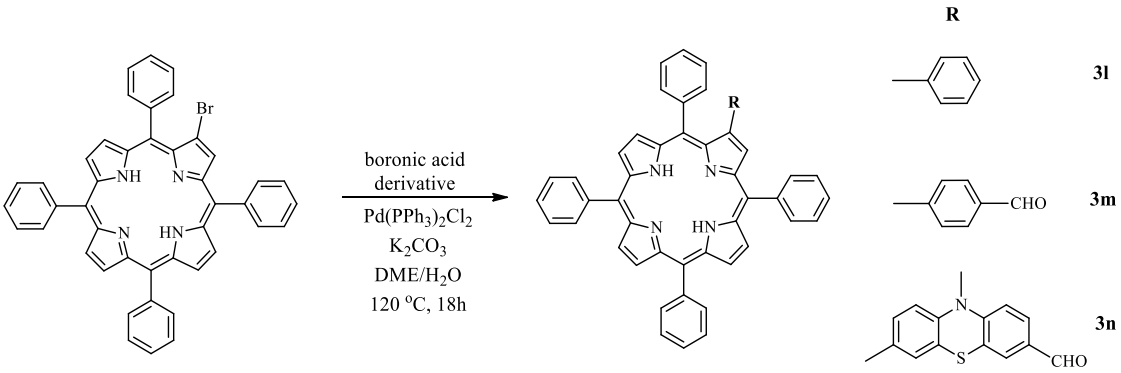

Scheme 17. Suzuki cross-coupling reaction of β-substituted porphyrin

The structure of new *meso*-and *β*-functionalized cross-coupling products was characterized by spectroscopic methods. In all cases, the ^{1}H-NMR spectra confirmed the proposed structure, while the unequivocal proton assignments were realized with COSY, HMQC and HMBS

experiments. The NMR spectra of metallo-coupling derivatives couldn't be recorded, due to the Zn(II)-MPP derivatives low solubility in deuterated solvents, such as $CDCl_3$-*d*, DMSO-d_6 or CDOD-d_6, but other spectroscopic methods (UV-Vis and HRMS analysis) demonstrated the synthesis of target compounds.

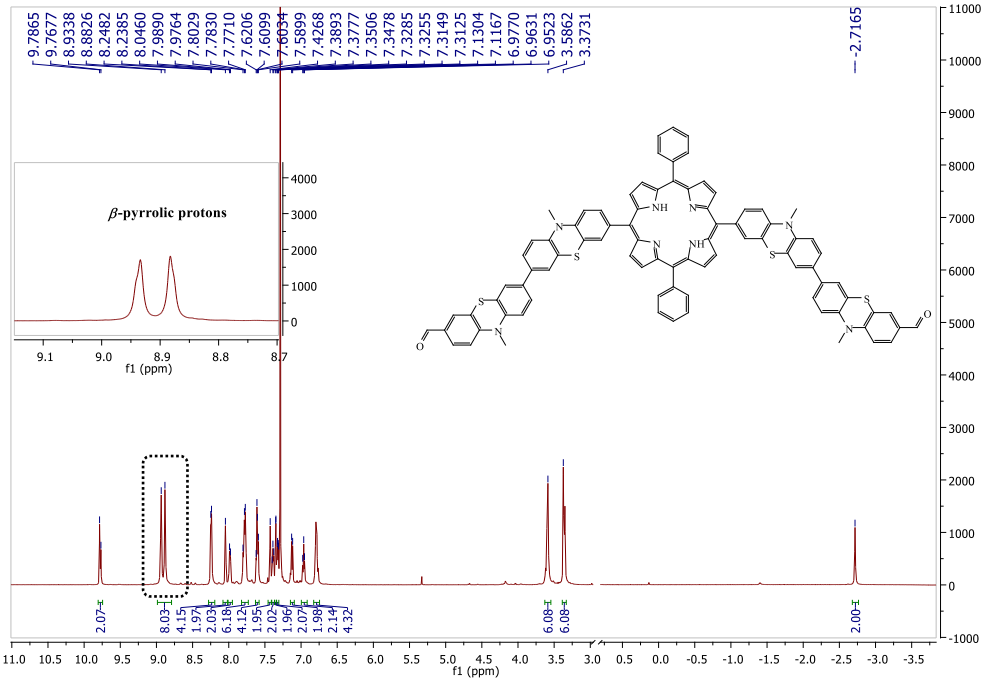

Figure 23. ^{1}H-NMR spectrum of A_2B_2-type meso-substituted-porphyrin ($CDCl_3$, 600MHz)

The ^{1}H-NMR spectra of MPP coupling products displayed a sharp singlet around -2.7 ppm corresponding to the two pyrrolenine nitrogens protons, followed by the next singlet peak analogous to the phenothiazine protecting methyl groups.

The aromatic region showed the all nonequivalent proton peaks, situated between 6.5-8.9 ppm. In case of the MPP coupling products bearing one or more formyl functional groups (**3a**, **3b**, **3e**, **3g**, **3i**, **3j**), the most deshielded singlets were the aldehyde protons, around 9.8 ppm, partially overlapped, owing to the similar chemical shifts.

In the spectra of *meso*-substituted porphyrins the eight pyrrolic protons appeared as a doublet with vicinal coupling constant of 4.6-5.2 Hz (*Figure 23*), while in the spectra of *β*-substituted-porphyrins only one multiplet was detectable with a total integration of seven protons corresponding to the pyrrolic hydrogens (*Figure 24*).

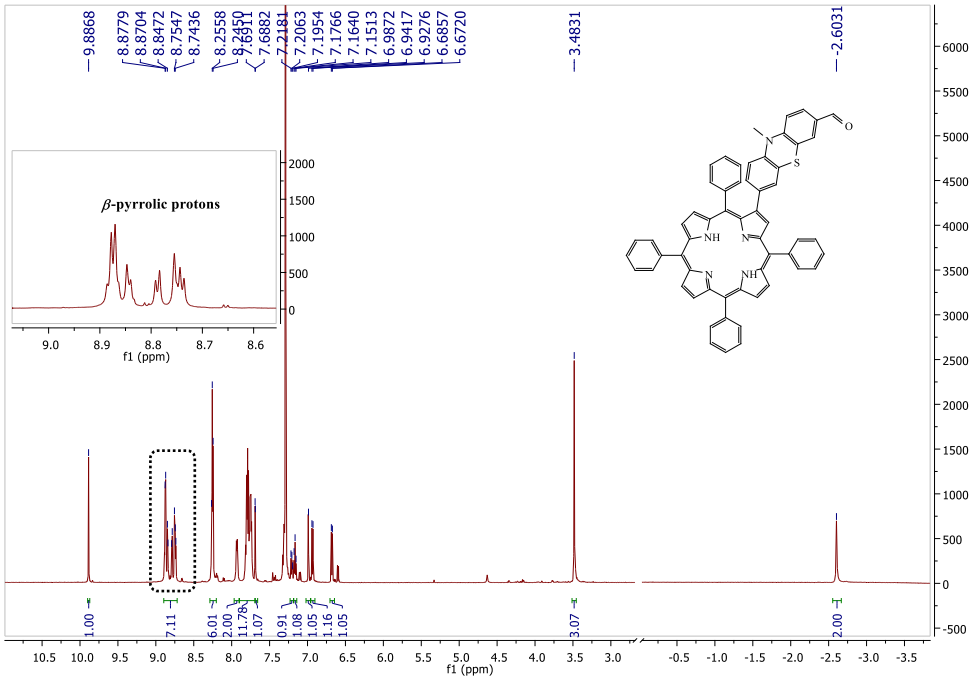

Figure 24. ^{1}H-NMR spectrum of β-substituted porphyrin ($CDCl_3$, 600MHz)

Optical properties of MPP cross-coupling products

The photophysical properties of MPP cross-coupling products were investigated by UV-Vis and fluorescence spectroscopic methods.

The UV-Vis absorption spectra were recorded in dichloromethane at 298 K and displayed the characteristic properties of free base and zinc-MPP derivatives. The absorption spectrum of each MPP presented a strong near-UV Soret band, located around 425 nm, and two or four (metallo- or free-base-MPP) low intensity Q bands situated in the visible spectral region at 515-655 nm. All the compounds are characterized by a dark purple color as a consequence of the intense absorption in the Soret band region. By examining the molar absorptivity values listed in Table 3, it can be seen that halogen-MPP **2e** and A_4 type *meso*-phenylene-bridged porphyrin-carbazole dyad **3c** appear well fitted for dyes applications, while the presence of the phenothiazine bridge in porphyrin-(hetero)aryl dyads **3f**-**3i** does not promote a hyperchromic effect.

Table 3. UV-Vis absorption maxima for halogen-MPP and cross-coupling products (in DCM solution)

Cpd	λ_{abs} [nm]		
	Ptz	Soret ε[M^{-1} cm^{-1}]	$Q_{4,3,2,1}$
2e	259	420 (369256)	517, 554, 592, 652
2g	259	421 (186680)	519, 555, 592, 651
2i	259	422 (134911)	519, 555, 592, 651
2k	257	422 (193193)	519,555, 598, 655
3f	259	422 (61409)	519, 555, 598, 655
Zn-3f	260	422 (58049)	548, 585
3g	250	420 (96961)	515, 555, 590, 650
3h	250	420 (79805)	515, 554, 590, 650
3d	250	418 (125483)	514, 552, 590, 655
Zn-3d	253	422 (72411)	548, 587
3e	245	420 (191988)	515, 555, 585, 645
3j	250	420 (78229)	520, 555, 590, 650
3k	245	420 (182215)	520, 555, 590, 650
3i	240	420 (95928)	520, 555, 590, 650
3b	-	423 (174035)	519, 548, 592, 652
3c	-	420 (660743)	515, 550, 590, 645
3a	-	427 (78383)	516, 555, 592, 642

The extended π-systems doesn't produce remarkable effects upon the absorption features of cross-coupling products, except for the **3j** compound, which showed a strong hyperchromic shift, due to the increasing number of electron-donating phenothiazine units (*Figure 25a*). In addition, the spectra of *β*-substituted-products showed an expanded Soret band as compared to the *meso*-substituted porphyrins (*Figure 25b*).

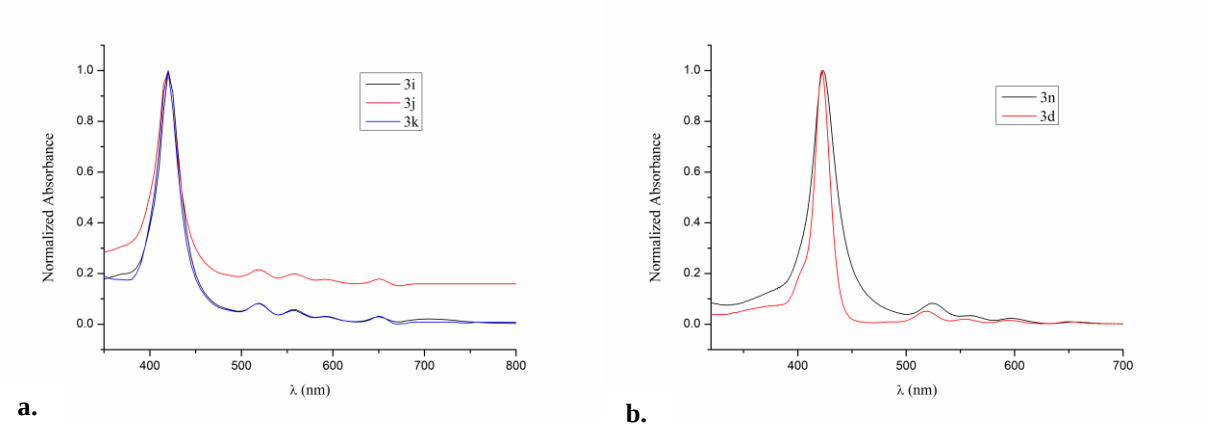

Figure 25. UV-Vis absorption spectra of meso- (a.) and β-substituted porphyrin (b.) (10^{-6} M in CH_2Cl_2)

The calculated molar extinction coefficient values ($mol^{-1}cm^{-1}$) of extended MPP derivatives **3h** (*660743*), **3i** (*191988)*, **3j** (*48480*), **3k** (*79850*), **3l** (*95928*), **3m** (*78229*), **3n** (*182214*) suggested them as suitable functional dyes candidates. The value of **3h** porphyrin was prominent, due to the four phenyl-carbazole chromophores attached to the porphyrin core.

The emission spectra of obtained porphyrins exhibited similar trend to the starting MPPs, dominated by two main features, the $Q_{(0,0)}$ and the $Q_{(0,1)}$ bands. Upon irradiation at the λ_{max} corresponding to Soret band, A_3B- and A_2B_2-type cross-coupling products showed red-orange daylight fluorescence, with remarkable Stokes shifts (4891-6565 cm^{-1}). *Figure 26a* illustrated a comparative emission spectrum of obtained compounds, and involved a large emission band (~660 nm) with a weak shoulder (~720 nm), which occurred from the asymmetric nature of these porphyrins.

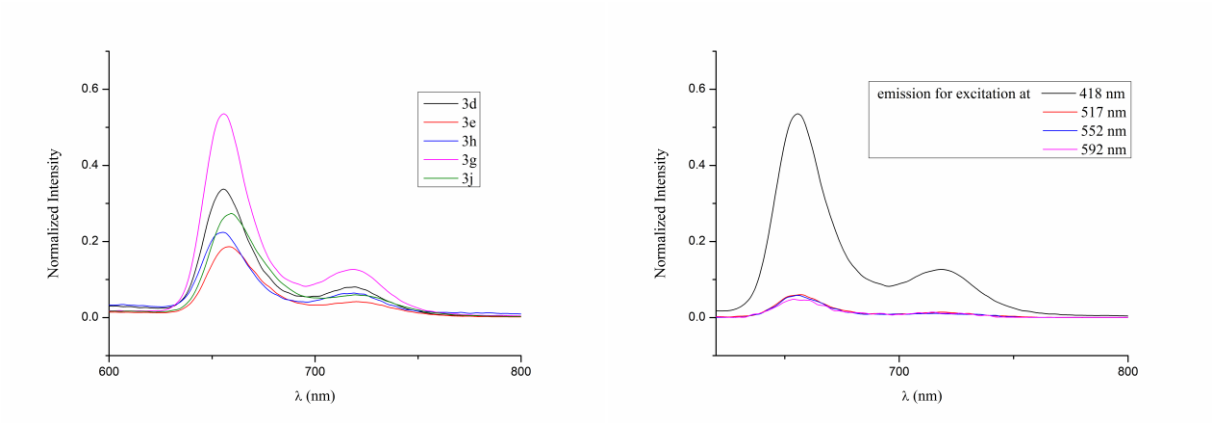

Figure 26. Fluorescence spectra of MPP cross-coupling products excited at λ_{Soret} (a.) and $\lambda_{Q\ bands}$ (b.) (10^{-7} M in CH_2Cl_2)

As we observed, the compound **3g** displayed the highest emission in solution, arose from the large conjugation between the phenothiazine and porphyrin chromophore units. *Figure 30* showed the emission spectra of **3g** upon excitation at four different wavelengths (Soret and Q bands). The excitations at λ_{max} corresponding to the Q_4 (517 nm), Q_3 (552 nm) and Q_2 (592 nm) resulted non-splitted low-intensity emission bands. The role of the phenothiazine units in dye skeleton may be considered as responsible on one hand for the energy dissipation by typical butterfly vibrations, generating low fluorescence emission in solution, but on the other hand, for enlarging the intermolecular distance due to its bent/butterfly structure, thereby preventing the intermolecular π–π stacking and subsequently stimulating fluorescence in the aggregated state. The parent MPP dyes displayed fluorescence emissions typical to the porphyrin core in 660–670

nm range, in solution, while the extension of the pending phenothiazine arms of A_3B type and A_2B_2 type MPP with supplementary peripheral phenothiazine or phenyl units resulted fluorescence quenching in compounds **3f**, and **3d**.

Table 4. Fluorescence emission spectral properties of the obtained phenothiazine-bridged porphyrin-(hetero)aryl dyads

Compounds	λ_{em}[a] [nm]	Stokes Shift [cm^{-1}]	ϕF[b]
3g	655	8542	0.16
3h	657	8588	0.14
3e	654	8519	0.18
3j	659	8635	0.19
3k	652	8472	0.08
3i	658	8612	0.15

a—excitation at $\lambda_{Soret,}$ *b*—quantum yields against TPP standard.

The presence of formyl auxochromic groups in peripheral positions appeared favorable by imparting molecular polarization, due to the electron withdrawing effect, and thus fluorescence emissions were recorded for compounds **3g**, **3e**, **3j** and **3i**, as shown in Table 4. Phenothiazine-bridged porphyrin-carbazole dyads A_3B type **3h** and A_2B_2 type **3k** presented fluorescence emissions in similar range. The symmetrical A_4 type phenylene-bridged porphyrin-(hetero)aryl dyads did not exhibit fluorescence emission regardless the nature of the peripheral units: phenyl-carbaldehyde **3a,** formyl-phenothiazine **3b** and N-phenyl carbazole **3c**.

3.2.3.2.Mizoroki-Heck cross-coupling products

The Heck coupling reaction between A_3B- and A_2B_2-type *meso*-substituted-porphyrins and vinyl-phenothiazine/ferrocene derivatives produced a series of new alkenyl-porphyrins in satisfactory yields.

Synthetic procedures

The synthesis of A_3B- and A_2B_2-type alkynyl-MPP derivatives were realized under standard Mizoroki-Heck coupling conditions. The palladium catalyst were obtained *in situ* by using $Pd(OAc)_2$ and PPh_3 ligand in DMF/toluene solvents mixture, which enhanced the solubility of porphyrins. The reaction of free-base/metallo-MPP and vinyl-phenothiazine/ferrocene derivatives resulted new coupling products (**4a**, **4b**, **4c**, **4d**, **Zn-4a**, **Zn-4b**, **Zn-4c**, **Zn-4d**) in moderate yield (~35%). The applied synthetic routes are presented in *Scheme 18.*

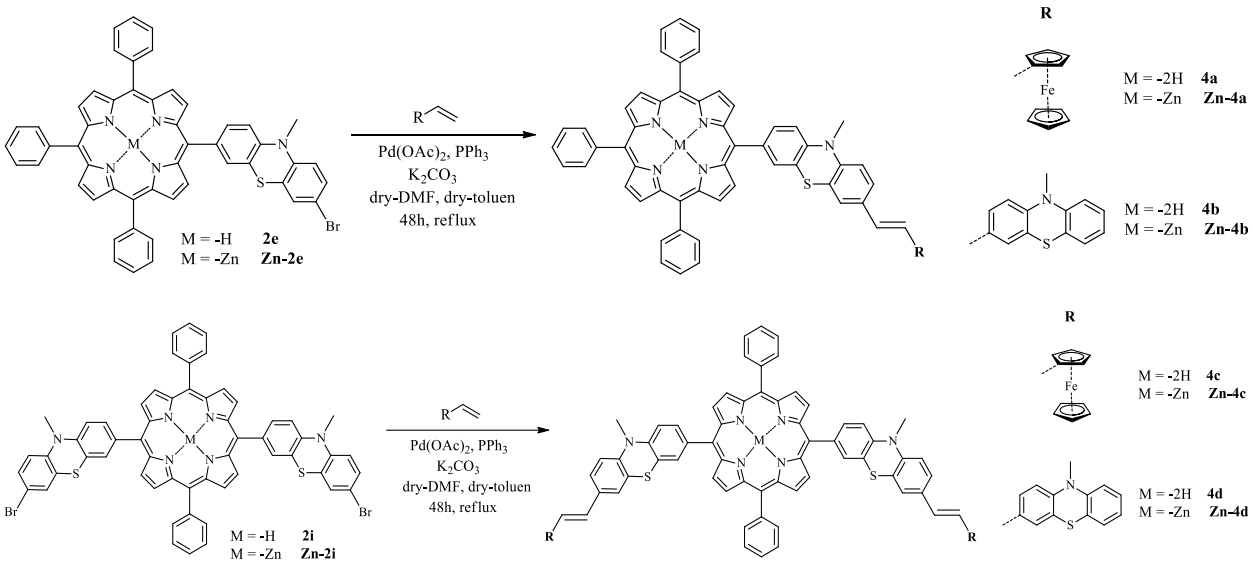

Scheme 18. Synthesis of A_3B- and A_2B_2-type vinyl-MPP derivatives

The structure of synthesized compounds was investigated by various spectroscopic techniques, including 1D-NMR (^{1}H, ^{13}C), 2D-NMR (COSY, HMQC, HMBC) and mass spectrometry (HRMS, APCI+). All porphyrins presented characteristic chemical shifts arising from *meso*-phenothiazine and phenyl protons, *β*-pyrrole protons, vinyl substituents protons and imine protons for free base derivatives.

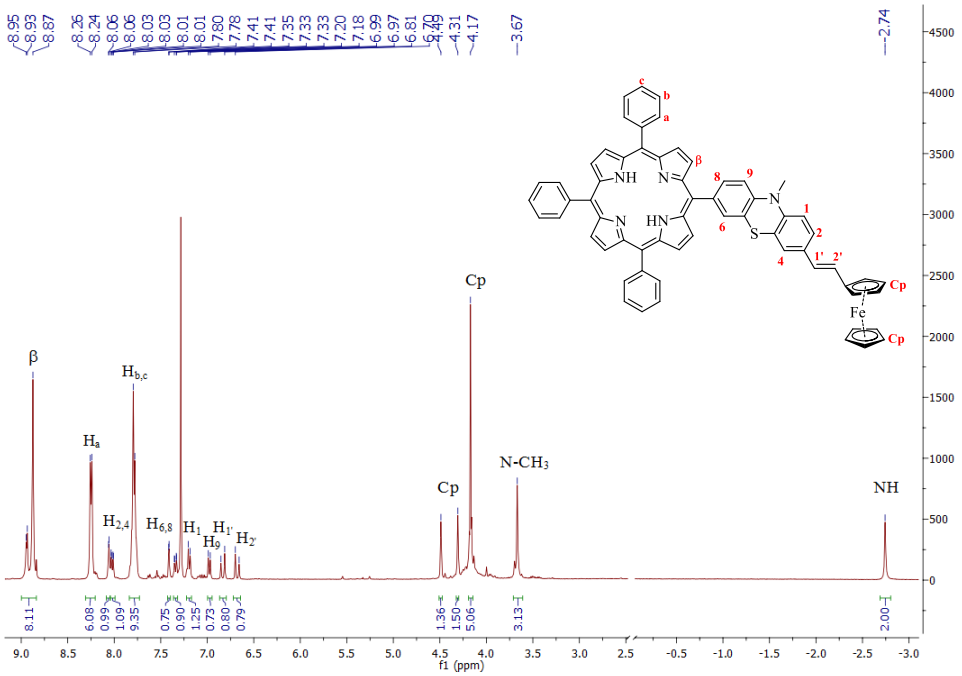

*Figure 27. ^{1}H-NMR spectrum of **4a** compounds ($CDCl_3$, 600 MHz)*

The ^{1}H-NMR spectra of alkynyl-porphyrins proved that all vinylene groups were in trans-conformation, due to the lack of peaks at 6.56 ppm which are typical for the protons in *cis*-double bond[142]. The ^{1}H-NMR spectrum of **4a** compound displayed the representative chemical shifts of the aliphatic and aromatic parts, and the integrated intensities were matching with the suggested structure. The signals of vinyl protons appeared at 6.70 and 6.81 ppm (with coupling constant of ^{3}J=16.0 Hz) and the inner pyrrolenine protons located at -2.74 ppm, certified the formation of *trans* isomer.

Optical properties of Heck-coupling products

The UV-Vis absorption spectra of A_3B- and A_2B_2-type free-base/metallo-vinyl-MPP derivatives indicated a slightly red-shifted Soret band (~424 nm) arising from the π–π* transitions within the extended π-systems, and two or four low-intensity Q bands in the 510-650 nm region, owing to the conjugation between the electron-withdrawing porphyrin and electron-donating ferrocene/phenothiazine-vinylene arms. As compared to the starting porphyrins, the obtained compounds with oligophenothiazine-vinylene arms (**4b**, **4d**, **Zn-4b**, **Zn-4d**) displayed a broadened Soret band with higher molar absorptivity, while the metallocene containing MPP derivatives (**4a**, **4c**, **Zn-4a**, **Zn-4c**) showed strong hypsochromic effect (*Figure 28*).

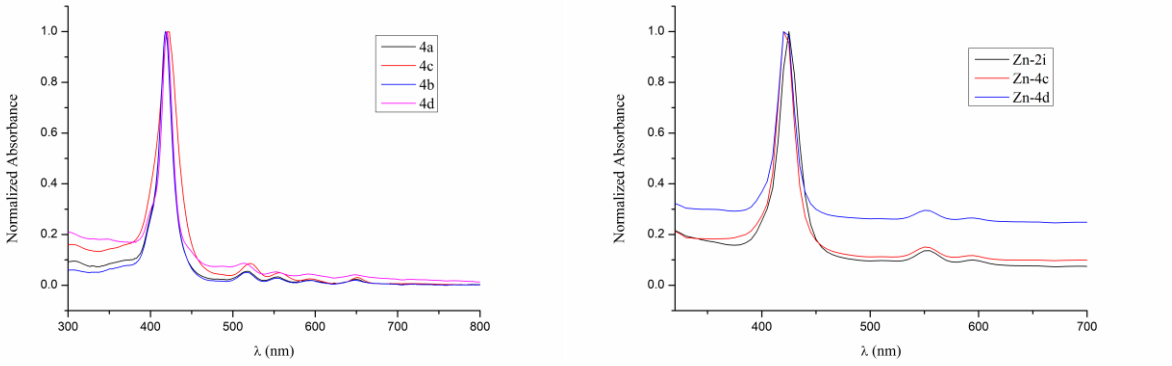

Figure 28. Normalized absorbance spectra of free-base- and metallo-vinyl-MPP derivatives (10^{-6} M in CH_2Cl_2)

The fluorescence spectra of vinyl-MPP derivatives presented a large emission band (~655 nm) with two weak shoulders (~600 and 720 nm), upon irradiation at the λ_{max} corresponding to Soret band. The appeared extra band between 550-600 nm was the most significant in case of A_2B_2-type MPP bearing ferrocene units (**4c**), and this phenomenon can be attributed to the strong

electronic "communication" between the phenothiazinyl-porphyrin π-system and the ferrocenyl moieties[143], as well as of their rich redox-switchable spectroscopic features[144].

Ferrocene/phenothiazine-porphyrin based donor-acceptor molecular architectures are highly interesting materials, due to their specific physic-chemical properties, such as generation of photocurrent, ability to create long-lived charge separated states. Owing to the attractive electronic and structural properties, the potential applications of these new compounds show great promise as molecular sensing tools (chemosensor)[145] or efficient artificial photosynthesis models[146]. All compounds displayed red-orange fluorescence with noticeable Stokes shift (8247-8679 cm^{-1}), but lower quantum yields (Φ_F = 0.05-0.06) as compared to the starting MPP derivatives. The fluorescence quantum yields were calculated against TPP as standard, using the known equation**Error! Bookmark not defined.**.

3.2.4. Biological Activity Evaluation of Phenothiazine-Bridged Porphyrin-Phenothiazine Dyad Fluorescent Dyes

Pursuing our goal of enabling the distinct visualization of human ovarian tumors, fluorescent dyes **3g**, **3i** and **3j** displaying fluorescence emission above 650 nm, in solution, and containing the carbaldehyde functional units prone to passing on the affinity towards the bio-materials were examined in vitro in terms of their cytotoxicity and their capacity for staining living cells by subcellular localization in human ovarian tumor A2780, cisplatin-resistant ovarian adenocarcinoma cells A2780cis and OVCAR-3 cell lines.

MTT Colorimetric Assay

The cells' viability was tested using the MTT colorimetric assay (dye 3-(4,5-dimethylthiazol-2-yl)-2,5-diphenyltetrazolium bromide) following a colorimetric protocol, reported previously[147]. Separate dilutions of each dye **3g**, **3i** and **3j** were employed in the treatment of ovarian adenocarcinoma cells lines under study. The modification in cell viability was observed by monitoring the concentration of the purple formazan formed after 24 h of incubation and displayed by the recorded optical density of the sample. The cells' viability was pronounced as percentage of survival in treated *versus* untreated cell populations. A close inspection proposed that there were no considerable differences between the cytotoxicity of the dyes **3g**, **3i** and **3j**, each of them showing a moderate toxicity on ovarian tumor cell lines in vitro (one-way analysis of variances,

Bonferroni post-test, in the 95% confidence interval). From the aspect of the cell's growth inhibition, A2780cis appeared the most resistant, while the folate receptor-rich OVCAR-3 cell line was the most reactive to being affected.

Cell Fluorescence Imaging

Fluorescence microscopy became an essential tool in single-molecule investigations, offering a high signal-to-noise ratio for visualization while still retaining the key features in the physiological context of native biological systems[148]. Fluorescent porphyrin macrocycles characterized by large Stokes shift between absorption (~400 nm) and red/NIR emission were explored in the fluorescence detection in various tissues or *in vivo*. To prevent the aggregation-caused quenching effect, one chemical approach was to introduce different bulky groups as substituents of the porphyrin core[149]. Fluorescence imaging was executed in order to investigate the internalization pathways of the selected fluorescent dyes **3g**, **3i** and **3j** inside the tested ovarian adenocarcinoma cells. In phenothiazine-bridged porphyrin-phenothiazine dyads A_3B type **3g** and A_2B_2 type **3j** the formyl group was attached to the "bowl-shaped" phenothiazine unit(s) prone to prevent the intermolecular π–π stacking, and green fluorescence was displayed by these staining agents in the aggregated state. Dye **3i** containing the formyl group attached to peripheral flat phenylene units exhibited aggregation-caused fluorescence quenching, due to π–π stacking aggregation favored by the planarity of the aromatic structure of the macrocycle, which limited its application.

The fluorescent dye concentration applied for cells staining was 50μM estimated and was well fitted for both fluorescence visualization and avoidance of cytotoxicity effects responsible for reducing the cell viability. Figure 29 illustrates the A2780cis cells in a typical Bright-field image (*Figure 29a*), their corresponding fluorescence imaging after the standard nuclei staining with DAPI (4′,6-diamidino-2-phenylindole) (*Figure 29b*), and fluorescence imaging after staining with fluorescent dye **3j** (*Figure 29c*).

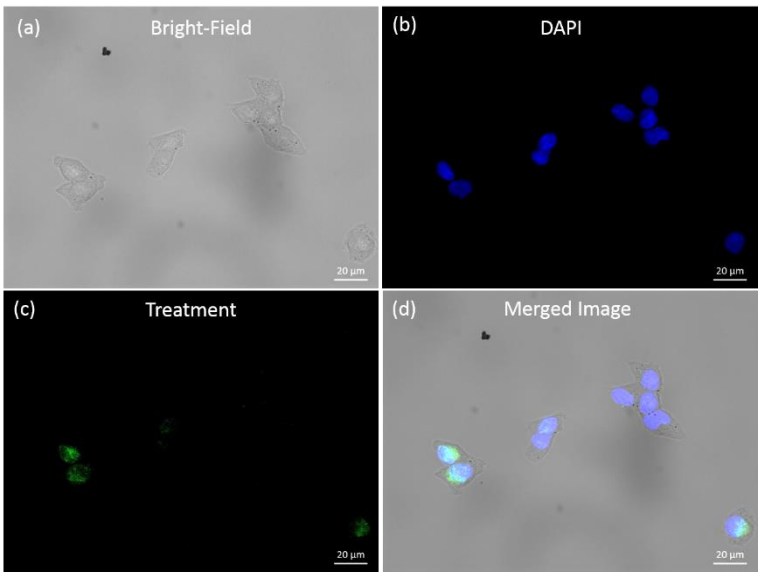

*Figure 29. Images of A2780cis cells: (a) Bright-field image. (b) Fluorescence images after staining with DAPI. (c) Fluorescence images after staining with **3j**. (d) merged fluorescence images (b) and (c).*

The merged fluorescence image presented in *Figure 29d* reveals the green fluorescent signal of dye **3j** overlain with the blue fluorescent signal of DAPI distributed inside the cells. This result allows us to conclude that fluorescent dye **3j** is able to accumulate both in the perinuclear and the nuclei region of the ovarian adenocarcinoma cells, being susceptible to crossing the nucleus membrane.

In order to confirm the cellular uptake of dye **3j**, we further invoked two photon excited-fluorescence lifetime imaging (TPE-FLIM), which is an ideal non-invasive technique for live-cell imaging, and offers multiple advantages over linear optical microscopy. The advantages of this technique including acquisition of fluorescence image with deep light penetration generated by NIR excitation, less photodamage of living organism and negligible background signal[150]. In recent literature, functional porphyrins were specified as potential fluorescent probes for TPE fluorescence imaging of various tumoral cells. Thus, 2-acetyl-6-dimethyl-aminonaphthalene–porphyrin dyads, characterized by intramolecular fluorescence resonance energy transfer process (FRET) from the aminonaphthalene donor to the porphyrin acceptor unit, were applied for TPE fluorescence imaging of lung cancer A549 cells under the irradiation with a 740 nm femtosecond laser[151,152]. Mesoporous silica nanocomposites containing the photosensitizer 5,10,15,20-tetrakis (1-methyl 4-pyridinio) porphyrin tetra (p-toluenesulfonate) were employed for targeted TPE-FLIM of human breast carcinoma cell line MCF-7 and the human lung cancer A549 cell line[153].

In our experiments, the selected wavelength of the excitation laser was 800 nm, ensuring that the combined energy of two photons spanned the gap between the ground state and first excited electronic state of the fluorescent dye **3j**. Figure 30 illustrates the bright field image corresponding to A 2780 cells (*Figure 30a*) and the TPE-FLIM image where the contrast is based on the lifetime of the fluorophore **3j** after staining A 2780 cells (*Figure 30b*).

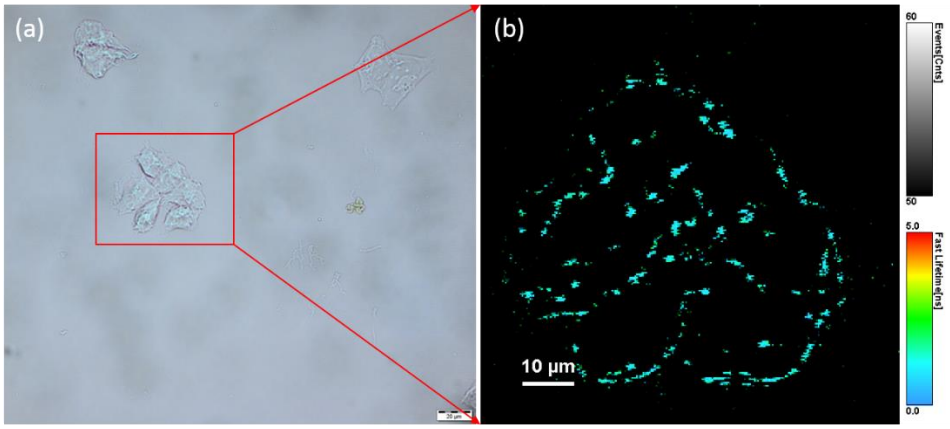

Figure 30. Microscopy imaging of A 2780 cells: (a) Bright-field image. (b) TPE-FLIM image after incubation for 24 h with dye 3j

The obtained TPE-FLIM image displays the successful molecular binding of the dye **3j** inside A2780 cells, giving the possibility of a distinct visualization of ovarian adenocarcinoma cells in NIR light.

3.2.5. Conclusions

In this part of thesis, a series of A_3B- and A_2B_2-type phenothiazinyl-porphyrin derivatives were prepared using different synthetic methods. Convenient one-pot procedure was applied for the synthesis of *meso*-MPP derivatives, containing up to four phenothiazinyl units linked to the porphyrin core (**2a**, **2b**, **2c**, **2d**, **2e**, **2f**, **2g**, **2h**, **2i**, **2j**, **2k**, **2l**, **2m**, **2n**, **2q**, **2r**, **2o**, **2p**, **2s**, **2t**, **2v**, **2w**, **2x**, **2y**).

The metal insertion into the central cavity of MPP macrocyclic systems was achieved by two-step methods. Thus, metallo-MPP derivatives were obtained by the treatment of previously presented free-base *meso*-phenothiazinyl-porphyrins with the corresponding bivalent metal (Zn, Pd, Ni, Cu) acetate in N,N-dimethylformamide solution at high temperature (**Zn-2e**, **Zn-2g**, **Zn-2i**, **Zn-2k**, **Pd-2e**, **Pd-2g**, **Pd-2i**, **Pd-2k**, **Ni-2e**, **Ni-2g**, **Ni-2i**, **Ni-2k**, **Cu-2e**, **Cu-2g**, **Cu-2i**, **Cu-2k**).

The peripheral modification by Suzuki-Miyaura cross coupling with different aryl-boronic acid derivatives afforded a series of *meso*-phenothiazine-bridged porphyrin-(hetero)aryl dyads in good yields (40-70%) (**3a**, **3b**, **3c**, **3d**, **3e**, **3f**, **3g**, **3h**, **3i**, **3j**, **3k**, **3l**, **3m**, **3n**, **Zn-3d** and **Zn-3f**). The Heck coupling reaction between A_3B- and A_2B_2-type *meso*-substituted-porphyrins and vinyl-phenothiazine/ferrocene derivatives produced a series of new alkenyl-porphyrins in satisfactory yields (**4a**, **4b**, **4c**, **4d**, **Zn-4a**, **Zn-4b**, **Zn-4c, Zn-4d**).

In the UV-Vis absorption spectra of novel MPP derivatives enhanced substituent effect was observed on absorption bands, due to the presence of electron-donating phenothiazine moiety: an intense band around 250 nm created by π-π^* transitions in the phenothiazine molecule[154], followed by a strong near-UV Soret band located at 425 nm and two (metallo-MPP) or four (free-base-MPP) low intensity *etio*-type Q bands situated in the visible spectral region (541-659 nm). The obtained new heterocyclic compounds displayed red-orange fluorescence with noticeable Stokes shift, but lower quantum yields, except for the case of **2q** which is an A_3B-type (trimethylsilyl)ethynyl-porphyrins and this property afforded an explicit evidence of efficient energy transfer processes by peripheral substitution with ethynyl groups.

The protonation study of MPP derivatives was realized in CH_2Cl_2 solution using trifluoroacetic acid (TFA) as the titrating agent. Upon stepwise addition of TFA the MPP macrocycles allowed for gain of two protons on the inner nitrogens to establish a dication (H_2MPP^{2+}) and increased the symmetry of porphyrin core (from D_{2h} to D_{4h} symmetry).

Upon protonation, the *meso*-phenothiazinyl-porphyrins presented substantial batochromic shift to an extent dependent on the peripheral substituents, allowing for the study of intensified light-harvesting properties in the red zone of the spectrum.

The distinct color change from brown to green may open new perspectives for potential applications as acid indicators for analytical purposes.

Furthermore, according to cell viability colorimetric assays (MTT and Alamar Blue), the phenothiazine-bridged porphyrin-phenothiazine dyads **3g**, **3i** and **3j** exhibit a moderate cytotoxicity on ovarian tumor cell lines *in vitro.*

The synthesized new MPP derivatives are fully characterized by 1D, 2D-COSY, 2D-HMQC and 2D-HMBC NMR spectroscopy, respectively HRMS spectrometry, using APCI or ESI ionization techniques.

4. General conclusions

The doctoral thesis presents the synthesis, structural characterizations and photophysical properties of 80 compounds, from various classes, including: N-alkyl-10*H*-phenothiazines and their formyl derivatives, N-alkyl-10*H*-phenothiazine-boronic acids, vinyl-phenothiaizne derivative, N-alkyl-10*H*-alkynyl-phenothiazine derivatives, N-alkyl-10*H*-alkynyl-bridge phenothiazinyl-phenyl aldehydes, *meso*-(hetero)aryl-porphyrins, *meso*-phenothiaznyl-porphyrins and their metal complexes, trimethylsilyl-ethynyl-porphyrins, arylethynyl-poprhyrins, phenothiazine-bridged porphyrin-(hetero)aryl dyads (by Suzuki-Miyaura) coupling reactions) and their metal complexes, vinyl-phenothiazinyl-porphyrin derivatives and their metal complexes.

From the 80 compounds 58 were synthesized and characterized for the first time in this thesis. Their photophysical properties, including UV-Vis linear and nonlinear absorption and fluorescence emissions are studied in solution and/or solid state.

10-alkyl-10*H*-phenothiazines (**1a-c**) and their formyl derivatives (**1d-h**) were successfully obtained in moderate to good yields with carefully selected reaction conditions. Bromo phenothiazine derivatives were converted to the corresponding phenothiazinyl boronic esters (**1j** and **1k**) through Pd-catalyzed borylation with bis(pinacolato) diboron as boron source.

For the synthesis of vinyl phenothiazine derivative (**1m**) a modified Wittig reaction was applied favorably. Furthermore, for the design of new triple carbon-carbon bonds between the halogenated phenothiazines and alkynes was realized by Sonogashira coupling reaction. Treatment of bromo-phenotiazine derivative with terminal alkynes in iPr_2NH/DMF in the presence of $PdCl_2(PPh_3)_2$ and CuI furnished the corresponding ethynyl-phenothiazine derivatives (**1o-s**).

Owing to this synthetic strategy, a series of phenothiazinyl based building blocks were prepared and were available for the synthesis and postfunctionalization of new phenothiazinyl-porphyrin derivatives.

The Adler-Longo mixed condensation reaction of 10-alkyl-10H-phenothiazine-carbaldehydes and/or other aromatic aldehydes with pyrrole afforded a mixture of AB_3- and A_2B_2-type of MPP (**2a-y**).

The family of *meso*-phenothiazinyl-phenyl-porphyrin MPP dyes was substantially extended by synthesizing the new halogen-MPP of AB_3- and *trans*-A_2B_2 type further employed, on the one hand, as ligands in new metal-complexes (**Zn**, **Pd**, **Ni** and **Cu** complexes), and on the other hand, as scaffolds for peripheral modification by Suzuki–Miyaura cross coupling with

various (hetero)arylboronic acid derivatives (**3a-n**). The cross-coupling methodology afforded a series of *meso*-phenothiazine-bridged porphyrin-(hetero)aryl dyads in good yields (40%–70%).

The examination of the UV–Vis optical properties of the newly synthesized compounds emphasized the absorption/emission properties of the porphyrin chromophore slightly modulated by the substitution pattern. The batochromic shift of the Soret band of all compounds can be attributed to the increasing number of electron-rich phenothiazine units in the *meso*-position as well as the presence of an intramolecular donor-acceptor molecular framework. In case of A_3B-type porphyrins higher molar absorptivity were observed in compared to the A_2B_2-types, due to the less symmetrical structure of compounds, which has been found to be a beneficial for broadening and red-shifting the absorption bands of porphyrin dyes.

Protonation studies of MPP derivatives were realized in CH_2Cl_2 solution using trifluoroacetic acid (TFA) as the titrating agent. Due to the increasing concentration of TEA (from 10μl to 100μl), the UV-Vis spectral changes of a free-base A_2B_2-type MPP (**2j**) presented a high intensity Soret band (red-shifted with 20 nm) and a large Q band, around 690 nm, with the occurrence of one isosbestic point. As compared to the corresponding free-base porphyrins, the most significant batochromic shifts (30 nm) were resulted in case of ethynyl-porphyrins (**2q**, **2v** and **2x**), due to the presence of ethynyl spacers, which ensured the electronic communication between the porphyrin core and the peripheral substituents. Upon protonation, both series of free-base and metallo-MPPs presented substantial batochromic shift to an extent dependent on the peripheral substituents, allowing for the study of intensified light-harvesting properties in the red zone of the spectrum.

In case of cross-coupling products the extended π-systems and the increasing size of the peripheral substituents did not produce remarkable effects upon the absorption features, except for the **3j** compound, which displayed a strong hyperchromic shift, due to the increasing number of electron-donating phenothiazine units. In addition, the spectra of *β*-substituted-products showed an expanded Soret band as compared to the *meso*-substituted porphyrins.

Based on the biological activity study, the green emissive dye **3j** can be successfully employed for living human ovarian tumor cell staining, at 50μM presenting a good cell internalization and having the capability to stain the cells' nuclei, without affecting the cell viability. Visualization of the stained cells can be performed both by TPE-FLIM and fluorescence imaging.

5. List of publications

Scientific publications:

E. Molnar, E. Gal, L. Gaina, C. Cristea, E. Fischer-Fodor, M. Perde-Schrepler, P. Achimas-Cadariu, M. Focsan, L. Silaghi-Dumitrescu, ***Novel Phenothiazine-Bridged Porphyrin-(Hetero)aryl dyads: Synthesis, Optical Properties, In Vitro Cytotoxicity and Staining of Human Ovarian Tumor Cell Lines,*** *International Journal of Molecular Sciences*, **2020**, 21, 3178.

E. Molnar, E. Gal, L. Gaina, C. Cristea, L. Silaghi-Dumitrescu, ***Ethyne Functionalized Meso-Phenothiazinyl-PhenylPorphyrins: Synthesis and Optical Properties of Free Base Versus Protonated Species,*** *Molecules*, **2020**, 25, 4546.

Conference presentations:

Functionalization reactions of new phenothiazinyl-porphyrins, 11th MatCatNet Workshop „From Molecules to Functionalised Materials", Ohrid, Macedonia, September 17-21, **2015**.

Functionalization of meso- and β-substituted porphyrin derivatives, XXI. International Conference on Chemistry, Csíksomlyó, Romania, September 23-27, **2015**.

Suzuki coupling reactions of meso-phenothiazinyl-porphyrins, ELTE Márton Áron Special College – PhD Conference, Debrecen, Hungary, March 4, **2016**.

Synthesis and characterization of phenothiazinyl-porphyrin derivatives with extended π-conjugation structures, XXIII. International Conference on Chemistry, Deva, Romania, October 25-28, **2017**.

Aryl-ethynyl-porphyrin derivatives: synthesis, characterization and photophysical properties, XXIV. International Conference on Chemistry, Sovata, Romania, October 24-27, **2018**.

Poster sections:

DIFFERENT FORMYLATION REACTIONS OF ARYL-PORPHYRINS, Éva-Andrea Molnár, Emese Gál, Luminiţa Silaghi-Dumitrescu, 12th MatCatNet Workshop „From Molecules to Functionalised Materials", Ohrid, Macedonia, September 1-5, **2016**.

NEW PHENOTHIAZINYL-PORPHYRIN BASED DENDRIMERS: DESIGN, SYNTHESIS AND PHOTOPHYSICAL PROPERTIES, Éva-Andrea Molnár, Emese Gál, Balázs Brem, Luminiţa Silaghi-Dumitrescu, II. Young Researchers' International Conference on Chemistry and Chemical Engineering, Budapest, Hungary, May 3-5, **2018**.

6. References

[1] K. Prakash, A. Z. Alsaleh, P. Rathi, , A. Sharma, M. Sankar, F. D'Souza, *ChemPhysChem*, **2019**, *20*, 2627.
[2] K. Zeng, W. Tang, C. Li, Y. Chen, S. Zhao, Q. Liu, Y. Xie, *J. Mater. Chem. A*, **2019**, *7*, 20854.
[3] S. Abu-Melha, *Arch. Pharm. Chem. Life Sci*, **2019**, *352*, e1800221.
[4] D. Sakow, B. Böker, K. Brandhorst, O. Burghaus, M. Böring, *Angew. Chem. Int. Ed.*, **2013**, *52*, 4912.
[5] R. Grisorio, B. Roose, S. Colella, A. Listorti, G. P. Suranna, A. Abate, *ACS Energy Lett.*, **2017**, *2*, 1029.
[6] M. A. Bakar, N. N. Sergeeva, T. Juillard, M. O. Senge, *Organometallics*, **2011**, *30*, 3225.
[7] E. Gal, B. Brem, I. Pereteanu, L. Gaina, T. Lovasz, M. Perde-Schrepler, C. Cristea, L. Silaghi-Dumitrescu, *Dyes Pigments*, **2013**, *99*, 144.
[8] G. Sudeshna, K. Parimal, *Eur. J. Pharmacol.*, **2010**, *648*, 6.
[9] S. Revoju, A. Matuhina, L. Canil, H. Salonen, A. Hiltunen, A. Abate, P. Vivo, *J. Mater. Chem.*, **2020**, *8*, 15486.
[10] J. P. Malrieu, B. Pullman, *Theor. Chim. Acta*, **1964**, *2*, 293.
[11] A. D. Mosnaim, V. V. Ranade, M. E. Wolf, J. Puente, M. A. Valenzuela, *Am. J. Ther.*, **2006**, *13*, 261.
[12] R. N. Ondarza, E. Hernandez, A. Iturbe, G. Hurtado, *Biotechnol. Appl. Biochem.*, **2000**, *32*, 61.
[13] M. J. Ohlow, B. Moosmann, *Drug Discov. Today*, **2011**, *16*, 119.
[14] Y. Zhang, C. E. Ballard, S.L. Zheng, X. Gao, et al., *Bioorg. Med. Chem. Lett.*, **2007**, *17*, 707.
[15] P. B. Madrid, W. E. Polgar, L. Toll, M. J. Tanga, *Bioorg. Med. Chem. Lett.*, **2007**, *17*, 3014.
[16] I. Mucsi, J. Molnar, N. Motohashi, *Int. J. Antimicrob. Agents*, **2001**, *18*, 67.
[17] S. Sharma, V. K. Srivastava, A. Kumar, *Pharmazie*, **2005**, *60*, 18.
[18] J. J. Aaron, M. D. Gaye Seye, S. Trajkovska, N. Motohashi, *Top. Heterocycl. Chem.*, **2009**, *16*, 153.
[19] S. Thokala, S. P. Singh, *ACS Omega*, **2020**, *5*, 5608.
[20] M. S. Kim, M. J. Cho, Y. C. Choi, K.-S. Ahn, et al., *Dyes Pigm.*, **2013**, *99*, 986.
[21] M. Mao, X. Zhang, L. Cao, Y. Tong, G. Wu, *Dyes Pigm.*, **2015**, *117*, 28.
[22] T. Singh, S. Sharma, V. K. Srivastava, A. Kumar, *Indian J. Chem.*, **2006**, *45*, 2558.
[23] O. M. Khdour, I. Bandyopadhyay, N. P. Visavadiya, S. R. Chowdhury, S. M. Hecht, *Med. Chem. Commun.*, **2018**, *9*, 1491.
[24] C. S. Kramer, K. Zeitler, T. J. J. Muller, *Tetrahedron Lett.*, **2001**, *42*, 8619.
[25] B. Nagarajan, S. Kushwaha, R. Elumalai, S. Mandal, et al., *J. Mater. Chem. A.*, **2017**, *5*, 10289.
[26] T. Hua, Z.-S. Huang, K. Cai, L. Wang, H. Tang, H. Meier, D. Cao, *Electrochim. Acta*, **2019**, *302*, 225.
[27] A. F. Buene, E. E. Ose, A. Zakariassen, A. Hagfeldt, B. Hoff, *J. Mater. Chem. A.*, **2019**, Accepted Manuscript.
[28]K. Pluta, B. Morak-Mlodawska, M. Jelen, *J. Heterocyclic Chem.*, **2009**, *46*, 355.
[29] S. Revoju, S. Biswas, B. Eliasson, G. D. Sharma, *Dyes Pigm.*, **2018**, *149*, 830.
[30] S. Revoju, S. Biswas, B. Eliasson, G. D. Sharma, *Org. Electron*., **2019**, *65*, 232.
[31] K. D. Theriault, T. C. Sutherland, *Phys. Chem. Chem. Phis.*, **2014**, *16*, 12266.
[32] Ng. Ph. Buu-Hoi, N. G. Hoan, *J. Chem. Soc*., **1951**, 1834.
[33] A. Vilsmeier, A. Haak, *Ber. Dtsch. Chem. Ges.*, **1927**, *60*, 119.
[34]Y. Hua, S. Chang, H. Wang, D. Huang, et al., *J. Power Sources*, **2013**, *243*, 253.
[35] A. R. Battersby, C. J. R. Fookes, G. W. J. Matcham, E. McDonald, *Nature (London)*, **1980**, *285*, 17.
[36] L. B. Josefsen, R. W. Boyle, *Theranostics*, **2012**, *2*, 916.
[37] W. Z. Kuster, *Physiol. Chem*., **1912**, *82*, 463.
[38] M. O. Senge, Y. M. Shaker, M. Pintea, C. Ryppa, et al., *Eur. J. Org. Chem.*, **2010**, 237.
[39] L. Z. B. Carrenho, C. G. Moreira, C. C. Vandresen, et al., *PhotodiagnosisPhotodyn. Ther*.,**2015**, *12*, 444.
[40] Y. Lv, L. Wu, W. Shen, J. Wang, G. Xuan, X. Sun, *J. Porphyr. Phtalocyanines*, **2015**, *19*, 769.
[41] H. Wei, R. Feng, Y. Fang, L. Wang, C. Chen, et al., *Chem. Eur. J.*, **2018**, *24*, 19341.
[42] Y. W. Li, J. H. Yao, X. S. Deng, X. X. Huang, *Mater. Sci. Forum*, **2011**, *663*, 616.
[43] M. Endo, M. Fujitsuka, T. Majima, *Chem. Eur. J.*, **2007**, *13*, 8660.
[44] J. Jiang, J. A. Spies, J. R. Swierk, A. J. Matula, et al., *J. Phys. Chem. C*, **2018**, *122*, 13529.
[45] O. Muller, V. Pichot, L. Merlat, L. Schmidlin, D. Spitzer, *Appl. Opt.*, **2016**, *55*, 3801.
[46] E. Fagadar-Cosma, Z. Dudas, M. Birdeanu, L. Almasy, *Mater. Chem. Phys.*, **2014**, *148*, 143.
[47] M. O. Senge, *Chem. Commun.*, **2011**, *47*, 1943.
[48] Z. Yao, J. Bhaumik, S. Dhanalekshmi, M. Ptaszek, P. A. Rodriguez, J. S. Lindsey, *Tetrahedron*, **2007**,*63*, 10657.
[49] J. S. Lindsey, *Acc. Chem. Res*., **2010**, *43*, 300.
[50] M. O. Senge, S. Plunkett, *ECS Transactions*, **2011**, *35*, 147.

[51] M. O. Senge, *Acc. Chem. Res.*, **2005**, *38*, 733.
[52] M. M. Pereira, C. J. P. Monteiro, A. Peixoto, *Targets in Heterocyclic Systems: Chemistry and Properties, Italian Society of Chemistry*, **2008**, 258.
[53]P. Rothmund, *J. Am. Chem. Soc.*,**1936**, *58*, 625.
[54]A. D. Adler, F. R. Longo, J. D. Finarelli, J. Goldmacher, J. Assour, L. J. Korsakoff, *J. Org. Chem.* **1967**, *32*, 476.
[55]J. S. Lindsey, I. C. Schreiman, H. C. Hsu, P. C. Kearney, A. M. Marguerettaz, *J. Org. Chem.* **1987**, *52*, 827.
[56] G. P. Arsenault, E. Bullock, S. F. MacDonald, *J. Am. Chem. Soc.* **1960**, *82*, 4384.
[57] T. D. Lash, *J. Eur. Chem.*, **1996**, *2*, 1197.
[58]Zs. Valicsek, O. Horvath, *Microchem. J.*, **2013**, *107*, 47.
[59] E. B. Fleischer, *Acc. Chem. Res.*, **1970**, *3*, 105.
[60] M. Biesaga, K. Pyrzynska, M. Trojanowicz, *Talanta*, **2000**, *51*, 209.
[61] E. B. Fleischer, J. H. Wang, J. *Am. Chem. Soc.*, **1960**, *82*, 3498.
[62] V. E. J. Walker, N. Castillo, C. F. Matta, R. J. Boyd, *J. Phys. Chem. A*, **2010**, *114*, 10315.
[63] J. A. Shelnutt, X. Z. Song, J. G. Ma, S. L. Jia, W. Jentzen, C. J. Medforth, *Chem. Soc. Rev.*, **1998**, *27*, 31.
[64]R. Harada, Y. Matsuda, H. Okava, R. Miyamoto, S. Yamauchi, T. Kojima, *Inorg. Chim. Acta*, **2005**, *358*, 2489.
[65]Z.-C. Sun, Y.-B.She, Y. Zhou, X.-F. Song, K. Li, *Molecules*, **2011**, *16*, 2960.
[66] A. Kumar, S. Maji, P. Dubey, G. J. Abhilash, S. Pandey, S. Sarkar, *Tetrahedron Lett.*, **2007**, *48*, 7287.
[67] A. D. Adler, F. R. Longo, F. Kampas, J. Kim, *J. Inorg. Nucl.Chem.*, **1970**, *32*, 2443.
[68](a) K. M. Smith, J. F. Unsworth, *Tetrahedron*, **1975**, *31*, 367; (b) M. O. Senge, K. M. Smith, *Photchem.Photobiol.*, **1991**, *54*, 841.
[69] M. Z. Mamardashvili, O. A. Golubchikov, *Russ. Chem. Rev.*, **2001**, *70*, 577.
[70] M. Gouterman, *J. Chem. Phys.*, **1959**, *30*, 1139.
[71] M. Gouterman, *J. Mol. Spectrosc.*, **1961**, *6*, 138.
[72] M. Gouterman, *J. Mol. Spectrosc.*, **1963**, *11*, 108.
[73] C. Weiss, H. Kobayashi, M. Gouterman, *J. Mol. Spectrosc.*,**1965**, *16*, 415.
[74] L. J. Prins, D. N. Reinhoudt, P. Timmerman, *Angew. Chem. Int. Ed.*, **2001**, *40*, 2382.
[75]K. M. Smith, *Porphyrins and Metalloporphyrins*, *Elsevier*, *Amsterdam*, **1975**, 910.
[76] M. Uttamlal, A. S. Holmes-Smith, *Chem. Phys. Lett.*,**2008**, *454*, 223.
[77] X. Huang, K. Nakanishi, N. Berova, *Chirality*, **2000**, *12*, 237.
[78] K. Tamao, T. Hiyama, E. Negishi, *J. Organomet. Chem.*, **2002**, *653*, 1.
[79] K. Bliss Fields, The Design and Synthesis of Functionalized Poprhyrins and Their Applications in Group Transfer Reactions, Medicine, and Materials, 2010, Graduate Theses and Dissertations.
[80] G. W. Parshall, S. Ittel, *Homogeneous Catalysis; Wiley-Interscience, New York*, **1992**, 356.
[81] S. Hiroto, Y. Miyake, H. Shinokubo, *Chem. Rev.*, **2017**, *117*, 2910.
[82] I. P. Beletskaya, A. V. Cheprakov, *Chem. Rev.*, **2000**, *100*, 3009.
[83] A. de Meijere, F. E. Meyer, *Angew. Chem., Int. Ed. Engl.*, **1995**, *33*, 2379.
[84] A. Suzuki, *Cross-Coupling Reactions of Organoboron Compounds with Organic Halides. Metal-Catalyzed Cross-Coupling Reactions, Wiley-VCH, Weinheim*, **1998**, 48.
[85] N. Miyaura, A. Suzuki, *Chem. Rev.*, **1995**, *95*, 2457.
[86] E. Negishi, X. Zeng, Z. Tan, M. Qian, Q. Hu, Z. Huang, *Palladium- or Nickel-Catalyzed Cross-Coupling with Organometals Containing Zinc, Aluminum, and Zirconium: The Negishi Coupling. Metal-Catalyzed Cross-Coupling Reactions, Wiley-VCH, Weinheim*, **2004**, 815.
[87] N. T. Mitchell, *Syntesis*, **1992**, *1992*, 803.
[88] K. Sonogashira, *J. Organomet. Chem.*, **2002**, *653*, 46.
[89] E. Negishi, L. Anastasia, *Chem. Rev.*, **2003**, *103*, 1979.
[90] R. Chinchilla, C. Najera, *Chem. Soc. Rev.*, **2011**, *40*, 5084.
[91] F. J. Hartwig, *Acc. Chem. Res.*, **2008**, *41*, 1534.
[92] D. S. Surry, S. L. Buchwald, *Angew. Chem. Int. Ed.*, **2008**, *47*, 6338.
[93] O. B. Locos, D. P. Arnold, *Org. Biomol. Chem.*, **2006**, *4*, 902.
[94] A. Suzuki, *J. Organomet. Chem.*, **1999**, *576*, 147.
[95] N. Miyaura, K. Yamada, A. Suzuki, *Tetrahedron Lett.*, **1979**, *20*, 3437.
[96] N. Miyaura, *Top. Curr. Chem.*, **2002**, *219*, 11.
[97] A. Suzuki, *J. Organomet. Chem.*, **2002**, *653*, 83.
[98] I. Maluenda, O. Navarro, *Molecules*, **2015**, *20*, 7528.
[99] C. Amatore, A. Jutand, G. Le Duc, *Chem.: Eur. J.*, **2011**, *17*, 2492.
[100]A. Suzuki, *Heterocycles*, **2010**, *80*, 15.

[101] J. V. Kingston, G. John, *J. Org. Chem.*, **2007**, *72*, 2816.
[102] D. Dolliver, B. T. Bhattarai, A. Pandey, M. L. Lanier, et al., *J. Org. Chem.*, **2013**, *78*, 3676.
[103] B. Saito, G. C. Fu, *J. Am. Chem. Soc.*, **2007**, *129*, 9602.
[104] C. Baillie, L. Zhang, J. Xiao, *J. Org. Chem.*, **2004**, *69*, 7779.
[105] J. Han, Y. Liu, R. Guo, *J. Am. Chem. Soc.*, **2009**, *131*, 2060.
[106] B. H. Lipshutz, T. B. Petersen, A. R. Abela, *Org. Lett.*, **2008**, *10*, 1333.
[107] R. F. Heck, *Org. React.*, **1982**, *27*, 345.
[108] D. E. Karakas, F. Durap, M. Aydemir, A. Baysal, *Appl. Organomet. Chem.*, **2016**, *30*, 193.
[109] C. M. Avila, J. S. Patel, Y. Reddi, M. Saito, et al., *Angew. Chem.. Int. Ed.*, **2017**, *56*, 5806.
[110] M. Miura, H. Hashimoto, K. Itoh, M. Nomura, *J. Chem. Soc., Perkin Trans. 1*., **1990**, 2207.
[111] A. de Meijere, F. E. Meyer, *Angew. Chem. Int. Ed. Engl.*, **1994**, *33*, 2379.
[112] I.P. Beletskaya, A. V. Cheprakov, *Chem. Rev.*, **2000**, *100*, 3009.
[113] D. Mc Cartney, P. J. Guiry, *Chem. Soc. Rev.*, **2011**, *40*, 5122.
[114] F. Ozawa, A. Kubo, T. Hayashi, *Chem. Lett.*, **1992**, *21*, 2177.
[115] X. Qiu, R. Lu, H. Zhou, X. Zhang, T. Xu, X. Liu, Y. Zhao, *Tetrahedron Lett.*, **2008**, *49*, 7446.
[116] Y. Lu, H. Song, X. Li, H. Agren, Q. Liu, J. Zhang, X. Zhang, Y. Xie, *Appl. Mater. Interfaces*, **2019**, *11*, 5046.
[117] R. Kumar, V. Sudhakar, K. Prakash, K. Krishnamoorthy, M. Sankar, *Appl. Energy Mater.*, **2018**, *1*, 2793.
[118] N. V. Krishna, J. V. S. Krishna, S. P. Singh, L. Giribabu, L. Han, I. Bedja, R. K. Gupta, A. Islam, *J. Phys. Chem. C*, **2017**, *121*, 6464.
[119] X. Qian, L. Lu, Y.-Z. Zhu, H.-H.Gao, J.-Y. Zheng, *RSC Adv.*, **2016**, *6*, 9057.
[120] J. Kralova, *Photochem. Photobiol*., **2006**, *82*, 432.
[121] A. Dudkowiak, E. Teslak, J. Habdas, *J. Mol. Struct*., **2006**, *93*, 792.
[122] S. Abu-Melha, *Arch. Pharm. Chem. Life Sci*., **2019**, *352*, e1800221.
[123]C. Bodea, V. Fărcăşan, I. Oprean, *Rev. Roum. Chim*., **1965**, *10(11)*, 1100.
[124]C. S. Kramer, K. Zeitler, T. J. J. Müller, *Org. Lett.*, **2000**, *2(23)*, 3723.
[125] X.-H. Zhang, S.-H. Choi, D. Choi, K.-H. Ahn, *Tetrahedron Lett.*, **2005**, *46*, 5273.
[126] L. Liu, Q. Guo, J. Li, B. Yao, W. Tian, *Chim. J. Chem*., **2013**, *31*, 456.
[127] C. S. Kramer, T. J. J. Muller, *Eur. J. Org. Chem.*, **2003**, *18*, 3534.
[128] P.K. Goldberg, T.J. Pundsack, K.E. Splan, *J. Phys. Chem. A*, **2011**, 115, 10452.
[129] Y. Zhan, Y. Xu, Z. Jin, W. Ye, P. Yang, *Dyes Pigm*., **2017**, *140*, 452.
[130] G Cauquill, M. A. Casadevall, *Bull. Soc. Chem. Fr.*, **1955**, *7-8*, 1061.
[131] J. Zhang, J.-Z. Zhang, H. B. Li, Y. Wu, Y. Geng, Z.-M. Su, *Phys. Chem. Chem. Phys.*, 2014, **16**, 24994.
[132] A. T. R. Williams, S. A. Winfield, J. N. Miller, *Analyst.*, **1983**, *108*, 1067.
[133] M. Vitasovic, M. Gouterman, H. Linschitz, *J. Porphyr. Phthalocyanines*, **2001**, *5*, 191.
[134] I. H. Wasbotten, J. Conradie, A. Ghosh, *J. Phys. Chem. B*, **2003**, *107*, 3613.
[135] H. Guo, J. Jiang, Y. Shi, Y. Wang, J. Liu, S. Dong, *J. Phys. Chem. B*, **2004**, *108*, 10185.
[136]H. Guo, J. Jiang, Y. Shi, Y. Wang, J. Liu, S. Dong, *J. Phys. Chem. B*, **2006**, *110*, 587.
[137] M. Gouterman, *The Porphyrins, Academic Press., New York*, **1978**, 3.
[138] G. De Luca, A. Romeo, L. M. Scolaro, *J. Phys. Chem. B*, **2006**, *110*, 14135.
[139] L. K. Hanson, W. A. Eaton, S. G. Sligar, I. C. Gunsalus, M. Gouterman, C. R. Connell, *J. Am. Chem. Soc*., **1976**, *98*, 2672.
[140] A. B. Rudine, B. D. Delfatti, C. C. Wamser, *J. Org. Chem.*, **2013**, *78*, 6040.
[141] C. Wang, C. C. Wamser, *J. Org. Chem.*, **2015**, *80*, 7351.
[142] T. Xu, R. Lu, X. P. Qiu, X. L. Liu, P. C. Xue, et al., *Eur. J. Org. Chem.*, **2006**, *17*, 4014.
[143] C. Bucher, C. H. Devillers, J. C. Moutet, G. Royal, E. Saint-Aman, *Coord. Chem. Rev.*, **2009**, *253*, 21.
[144] A. Vecchi, P. Galloni, B. Floris, V. N. Nemykin, *J. Porphyr. Phtalocyanines*, **2013**, *17*, 165.
[145] C. Bucher, C. H. Devillers, J. C. Moutet, J. Pecaut, et al., *Dalton Trans.*, **2005**, *22*, 3620.
[146] D. M. Guldi, H. Imahori, *J. Porphyr. Phtalocyanines*, **2004**, *8*, 1410.
[147] B. A. Bocsa, A. Ilea, O. Soritau, C. tatomir, N. Miklasova, A. E. Mihu, C. M. Mihu, C. S. Melincovici, E. Fischer-Fodor, *Eur. J. Oral. Sci*, **2019**, *127*, 304.
[148] S. Shashkova, M. C. Leake, *Biosci. Rep*., **2017**, *37*, 37.
[149] Q. Yu, S. Chen, C. Han, H. Guo, F. Yang, *J. Lumin.*, **2020**, *220*, 117017.
[150] A. Khadria, J. Fleischhauer, I. Boczarow, J. D. Wilkinson, M. Kohl, H. L. Anderson, *iScience*, **2018**, *4*, 153.
[151] M. Zhu, C. Su, P. Xing, Y. Zhou, L. Gong, J. Zhang, H. Du, Y. Bian, J. Jiang, *Inorg. Chem. Front*, **2018**, *5*, 3061.
[152] M. Zhu, J. Zhang, Y. Zhou, P. Xing, L. Gong, C. Su, D. Qi, H. Du, Y. Bian, J. Jiang, *Inorg. Chem.*, **2018**, *57*, 11537.

[153] S. Lia, Y. Zhanga, X.-W. Hea, W.-Y. Li, Y.-K. Zhangab, *Talanta*, **2020**, *209*, 120552.
[154] G Cauquill, M. A. Casadevall, *Bull. Soc. Chem. Fr.*, **1955**, *7-8*, 1061.